

Inference-time Scaling of Diffusion Models through Classical Search

Xiangcheng Zhang¹Haowei Lin¹Haotian Ye²James Zou²Jianzhu Ma¹Yitao Liang¹Yilun Du^{3*}¹Helixon US Inc. ²Stanford University ³Harvard University

Abstract

Classical search algorithms have long underpinned modern artificial intelligence. In this work, we tackle the challenge of inference-time control in diffusion models—adapting generated outputs to meet diverse test-time objectives—using principles from classical search. We propose a general framework that orchestrates local and global search to efficiently navigate the generative space. It employs a theoretically grounded local search via annealed Langevin MCMC and performs compute-efficient global exploration using breadth-first and depth-first tree search. We evaluate our approach on a range of challenging domains, including planning, offline reinforcement learning, and image generation. Across all tasks, we observe significant gains in both performance and efficiency. These results show that classical search provides a principled and practical foundation for inference-time scaling in diffusion models. Project page at diffusion-inference-scaling.github.io.

1 Introduction

Classical search algorithms have laid the foundation for modern artificial intelligence [58]. In discrete settings, graph search algorithms are widely used to explore the state space. Breadth-first search (BFS) [50] and depth-first search (DFS) [72] traverse the search tree in a fixed order. To better leverage problem-specific information, best-first search methods [56], such as A* [24], use a heuristic to evaluate and prioritize states. Alternatively, local search methods, such as hill-climbing [58, Sec. 4.1], explore neighboring states. More recent techniques like gradient descent and Markov Chain Monte Carlo (MCMC) have become widely adopted in optimization and probabilistic inference, underpinning many modern AI models.

Diffusion models [26] have shown impressive performance in generative modeling for continuous domains such as images [12], videos [28], and world modeling [92]. They are also increasingly used in robotics and decision-making [43, 5, 73] to generate diverse actions [10]. However, generated samples may not always align with physical laws [66] or human intent [78], and the vast generative space often necessitates multiple trials to produce satisfactory outputs [87]. To address this, we scale up *inference-time compute* using strategic search methods that navigate the generative manifold for high-quality samples. We formalize sample evaluation using a verifier function $f(x_0)$ defined on *ground truth* samples, which measures the quality of the sample. Such verifiers could be reward functions [89], Q-functions [44], classifier conditions $p(c|x_0)$ [94, 12], and multi-modal LLMs [29].

To efficiently search the generative space induced by diffusion, we revisit classical search principles. Inspired by local search, when the verifier f is differentiable, we use Langevin MCMC to explore

*Corresponding author. Contact ydu@seas.harvard.edu

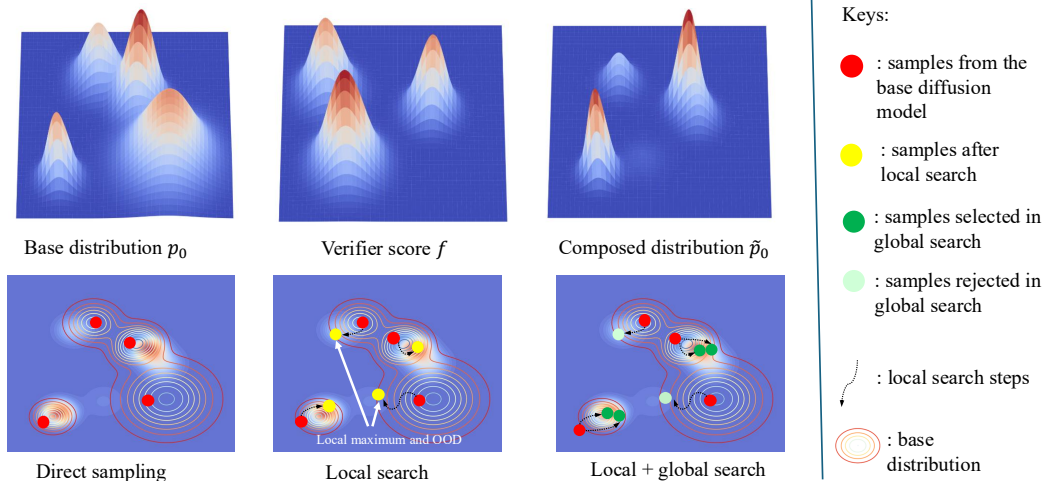


Figure 1: **Illustration of our search framework.** **Bottom left:** direct sampling results in samples with low verifier scores. **Bottom middle:** Local search navigates samples to nearby high-score regions, but suffers from local maximums and OOD samples. **Bottom right:** introducing global search explores diverse modes globally, allocating more compute to high-quality samples, and sampling from global optimal modes.

neighborhoods of current samples, guided by the verifier gradient and “score function” [77] from the diffusion model. To explore diverse modes in the complex distribution generated by diffusion models, we search the Markov chain of the “denoising process” with global search methods. Viewing sampling as a search tree, we use BFS and DFS to gradually explore the states while denoising. Like best-first search methods, we can evaluate intermediate states \mathbf{x}_t using the verifier $f(\mathbf{x}_{0:t})$, expanding high-quality paths more effectively. An illustration of local and global search is shown in Fig. 1.

Recently, Ma et al. [48] also explored inference-time scaling of diffusion models using search-based techniques, focusing on image generation tasks. Their zero-order search approach can be interpreted as an instance of local search, while their path-based strategies a combination of both local and global search. However, their method does not effectively leverage verifier gradients, and we introduce a local search strategy with annealed Langevin MCMC, efficiently steering sampling toward high-score regions. Moreover, we systematically evaluate the compute efficiency of search methods. Finally, we extend inference-time scaling beyond image generation to a broader set of domains.

To this end, we summarize our key contributions as follows:

- i) We propose a general and unified framework for efficient inference-time search in diffusion models, drawing inspiration from classical search algorithms. Specifically, we introduce a local search method based on Langevin MCMC that theoretically unifies prior gradient-based approaches, and we develop efficient global search strategies using tree-based algorithms such as BFS and DFS.
- ii) We implement inference-time scaling across a range of tasks—including planning, offline reinforcement learning, and image generation—and introduce task-specific verifiers. Our results demonstrate that inference-time scaling with search against verifiers can significantly improve the performance on many downstream tasks. Throughout the experiments, we show that our proposed approaches consistently surpass baselines in terms of compute efficiency.

2 Related Works

Here we provide a brief overview of inference-time scaling and diffusion models. For a more in-depth literature review see Appendix. B.

Scaling inference-time compute has its roots in cognitive science, often associated with “System 2” thinking [32, 3]. Yao et al. [93] conceptualize problem-solving in large language models (LLMs) as a combinatorial tree search problem [52, 53], proposing the Tree-of-Thoughts framework, which leverages breadth-first and depth-first search for more efficient reasoning.

Inference-time scaling has recently shown impressive performance with LLMs in reasoning and problem-solving tasks. For instance, [30, 76] train models to generate long chain-of-thought (CoT) [81], while others such as [64, 85] incorporate process reward models [39] to guide the generation process more effectively. These works focus on efficient exploration in discrete search spaces, often employing global search strategies. In contrast, diffusion models operate in a continuous, multimodal generative space. Furthermore, the autoregressive nature of LLMs allows for efficient evaluation of intermediate generation steps—something not directly feasible in diffusion models [12, 44].

Inference-time scaling for diffusion models remains relatively underexplored. Recent works such as [48, 51] introduce BFS-style global search algorithms, resampling candidate samples (or “particles”) at each noise level based on verifier scores (potentials). However, these methods do not effectively perform local search. Alternatively, Du et al. [15] propose learning a series of annealed energy landscapes and applying Langevin MCMC for iterative refinement. In this work we propose a general principled framework, encompassing prior methods as instances of local search and global search.

3 Backgrounds

3.1 Diffusion Probabilistic Models

Suppose we have D -dimensional random variable $\mathbf{x}_0 \in \mathbb{R}^D$ with distribution $p_0(\mathbf{x}_0)$. Diffusion models [26, 65] and the more general flow models [41, 2] are generative models that turn noise into data via a stochastic process $\{\mathbf{x}_t\}_{t=0}^T$. The forward “noising” process with $t > s$ can be defined as:

$$q(\mathbf{x}_t|\mathbf{x}_s) = \mathcal{N}\left(\mathbf{x}; \frac{\alpha_t}{\alpha_s}\mathbf{x}_s, \alpha_t^2\left(\frac{\sigma_t^2}{\alpha_t^2} - \frac{\sigma_s^2}{\alpha_s^2}\right)\mathbf{I}\right). \quad (1)$$

where α_t, σ_t are referred as the noise schedule with $\alpha_0 = \sigma_T = 1, \alpha_T = \sigma_0 = 0$. We can thus write the random variables \mathbf{x}_t as an interpolation between data and noise [47]:

$$\mathbf{x}_t = \alpha_t\mathbf{x}_0 + \sigma_t\epsilon,$$

and denote $q_t(\mathbf{x}_t)$ as the marginal distribution of \mathbf{x}_t . To model the reverse “denoising” process, we train the model using the denoising objective [26]:

$$L(\theta) = \mathbb{E}_{t, \mathbf{x}_0, \epsilon} [\epsilon_\theta(\mathbf{x}_t, t) - \epsilon],$$

which is equivalent of learning the score function of $q_t(\mathbf{x}_t)$ [77], as the ground truth of $\epsilon_\theta(\mathbf{x}_t, t)$ is $-\sigma_t \nabla_{\mathbf{x}_t} \log q_t(\mathbf{x}_t)$. To generate samples, we transform noise into data via the reverse transition kernel $p_\theta(\mathbf{x}_{t-1}|\mathbf{x}_t)$. In practice, we either sample \mathbf{x}_{t-1} using deterministic samplers like DDIM [65]:

$$\mathbf{x}_{t-1} = \frac{\alpha_{t-1}}{\alpha_t}(\mathbf{x}_t - \sigma_t\epsilon_\theta(\mathbf{x}_t, t)) + \sigma_{t-1}\epsilon_\theta(\mathbf{x}_t, t)$$

or stochastic samplers like DDPM [26, 54]:

$$p_\theta(\mathbf{x}_{t-1}|\mathbf{x}_t) = \mathcal{N}(\mathbf{x}_{t-1}; \boldsymbol{\mu}_\theta(\mathbf{x}_t, t), \boldsymbol{\Sigma}_\theta(\mathbf{x}_t, t)).$$

3.2 Compositional and Controllable Generation of DPMs

Given a base diffusion model with data distribution $p_0(\mathbf{x}_0)$, one may wish to sample \mathbf{x}_0 with some constraints or conditions $f(\mathbf{x}_0)$. Exact diffusion sampling from the composed distribution $\tilde{p}_0(\mathbf{x}_0) \propto p_0(\mathbf{x}_0)f(\mathbf{x}_0)$ would require training a time-dependent f on data generated by p_0 [12, 44], which may not be applicable in practice. Thus, we adopt optimization based methods to approximate the target distribution.

Compositional generation via annealed Langevin MCMC. When sampling from a compositional distribution composed of multiple probability distributions, $\tilde{p}_0(\mathbf{x}_0) \propto p_0(\mathbf{x}_0)\tilde{p}_0(\mathbf{x}_0)$, [14] proposes annealed Langevin MCMC sampling. In this approach, a sequence of annealed distributions $\tilde{q}_t(\mathbf{x}_t) \propto q_t(\mathbf{x}_t)\hat{q}_t(\mathbf{x}_0)$ is constructed, and samples are drawn using Langevin dynamics [82]:

$$\mathbf{x}_t^{i+1} = \mathbf{x}_t^i + \eta \nabla_{\mathbf{x}} \log \tilde{q}_t(\mathbf{x}_t^i) + \sqrt{2\eta}\epsilon^i, \quad \epsilon^i \sim \mathcal{N}(\mathbf{0}, \mathbf{I}). \quad (2)$$

Since the distribution of \mathbf{x}_t^i converges to $\tilde{q}_t(\mathbf{x}_t)$ asymptotically as $i \rightarrow \infty, \eta \rightarrow 0$, we can sample from $\tilde{p}_0(\mathbf{x}_0)$ following the annealing path $\{\tilde{q}_t\}_{t=0}^T$ with $\tilde{q}_0 = \tilde{p}_0$. Moreover, since the score of \tilde{q}_t can be directly computed by composing the score of two distributions:

$$\nabla_{\mathbf{x}} \log \tilde{q}_t(\mathbf{x}_t) = \nabla_{\mathbf{x}} \log q_t(\mathbf{x}_t) + \nabla_{\mathbf{x}_t} \log \hat{q}_t(\mathbf{x}_t),$$

thus do not require extra training.

Controllable generation through training-free guidance. During the sampling process, training-free guidance propose to update \mathbf{x}_t using gradient ascent

$$\tilde{\mathbf{x}}_t = \mathbf{x}_t + \Delta_t, \quad \Delta_t = \rho_t \nabla_{\mathbf{x}_t} \log f(\mathbf{x}_{0|t}) + \mu_t \alpha_t \nabla_{\mathbf{x}_{0|t}} \log f(\mathbf{x}_{0|t}). \quad (3)$$

where $\mathbf{x}_{0|t} = \mathbb{E}[\mathbf{x}_0 | \mathbf{x}_t] = \frac{\mathbf{x}_t - \sigma_t \epsilon_{\theta}(\mathbf{x}_t, t)}{\alpha_t}$. This method approximates the intractable posterior with the posterior mean: $\mathbb{E}_{\mathbf{x}_0 | \mathbf{x}_t} [f(\mathbf{x}_0)] \approx f(\mathbb{E}[\mathbf{x}_0 | \mathbf{x}_t])$. To enhance the guidance strength, [95] propose to apply a recurrence strategy, which first samples \mathbf{x}_{t-1} via $p_{\theta}(\mathbf{x}_{t-1} | \mathbf{x}_t)$, add the guidance gradient, then add noise back to \mathbf{x}_t through the forward process $q_t(\mathbf{x}_t | \mathbf{x}_{t-1})$:

$$\mathbf{x}_{t-1}^i \sim p_{\theta}(\cdot | \mathbf{x}_t^i), \quad \tilde{\mathbf{x}}_{t-1}^i = \mathbf{x}_{t-1}^i + \frac{\alpha_{t-1}}{\alpha_t} \Delta_t, \quad \mathbf{x}_t^{i+1} \sim q_t(\cdot | \tilde{\mathbf{x}}_{t-1}^i), \quad i = 1, 2, \dots, N_{\text{recur}}, \quad (4)$$

with N_{recur} being the total number of recurrence steps.

4 Methods

Problem Formulation. Given a pretrained diffusion model $\epsilon_{\theta}(\mathbf{x}_t, t)$ with a base distribution $p_0(\mathbf{x}_0)$, at test-time, we often wish to optimize the generation process to satisfy task-specific objectives. For instance, in reinforcement learning, this might involve generating high-value actions; in image synthesis, we may seek images that satisfy certain constraints such as color or shape; and in trajectory generation, we may want the outputs to conform to physical laws. In this paper, we are interested in how to scale test-time inference to follow such objectives.

We consider an inference-time scaling strategy that adjusts the sampling process based on a verifier function. Specifically, we define a verifier $f(\mathbf{x}_0) : \mathbb{R}^D \rightarrow \mathbb{R}^+$ which specifies the degree to which samples optimize a specified objective. We then aim to bias sampling toward regions of the sample space where $f(\mathbf{x}_0)$ is high. This leads to the objective of sampling from a compositional distribution that combines the original model distribution with the verifier:

$$\tilde{p}_0(\mathbf{x}_0) \propto p_0(\mathbf{x}_0) f(\mathbf{x}_0)^{\lambda},$$

where λ controls the weight of verifier scores.

Since exact sampling from the distribution is often impractical, we aim to search the manifold for the target samples at *inference time*, both *locally* and *globally*. First, we search the vicinity of the sample using hill-climbing style local search methods, guided by the verifier gradient. However, local search may stuck in a local maximum, where we then propose global graph search algorithms to explore the diverse modes in the complex generative landscape of diffusion models.

4.1 Local Search via Langevin MCMC with Verifier Gradient

To sample from the composition distribution \tilde{p}_0 , we conduct local-search with hill-climbing methods, aiming to find the local maximum with high \tilde{p}_0 . Specifically, we view the sampling problem as compositional optimization in measure space [83], and follow the gradient flow of KL-divergence, performing Langevin MCMC steps (details see Appendix. C.1).

Similar to annealed Langevin MCMC in [14], we could construct a series of annealed functions $\hat{f}_t(\mathbf{x}_t)$ with $\hat{f}_0(\mathbf{x}_0) = f(\mathbf{x}_0)$. Then we sample from the distributions $\tilde{q}_t(\mathbf{x}_t) \propto q_t(\mathbf{x}_t) \hat{f}_t(\mathbf{x}_t)$ through Langevin MCMC in Eq. 2 (details see Appendix. C.2). However, it remains unclear how to design such annealed verifier functions $\hat{f}_t(\mathbf{x}_t)$ efficiently, especially without training. Alternatively, training-free guidance in Eq. 3 utilizes the gradient of $f(\mathbf{x}_{0|t})$ to optimize \mathbf{x}_t , which can be computed directly using the diffusion model output. However, naive gradient updates have been observed to produce OOD and adversarial samples [60]. In [94], recurrence (Eq. 4) was found to help avoid adversarial samples in challenging guidance tasks, though its theoretical underpinnings remain poorly understood. We unify these two approaches by demonstrating that training-free guidance with recurrence, in the continuous limit, constitutes an instance of Langevin MCMC. For details see Appendix. C.3.

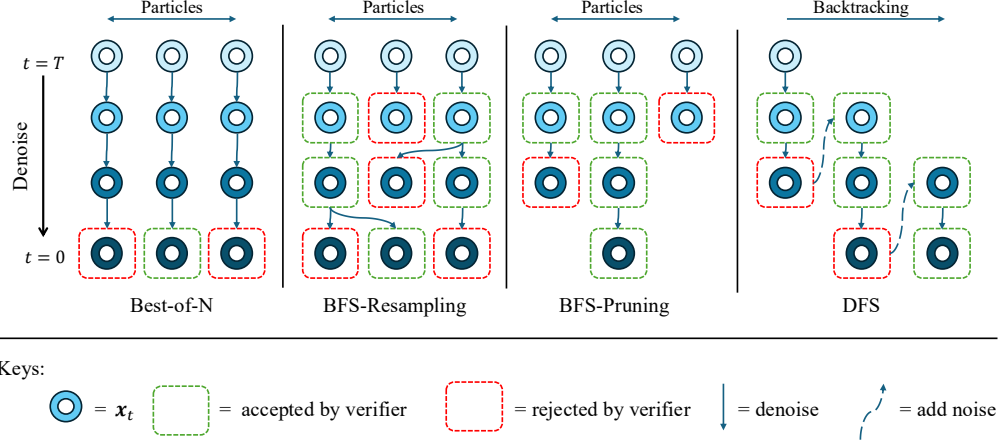


Figure 2: **Illustration of global tree search algorithms.** **Left:** Best-of-N sampling denoises multiple samples in parallel and selects the one with the highest verifier score at the final step. **Middle Left:** BFS-Resampling resamples particles at intermediate noise levels, allocating more children to nodes with higher scores. **Middle Right:** BFS-Pruning removes particles with low verifier scores during denoising, sampling at most one child per node. **Right:** DFS denoises a single particle until its verifier score violates the constraint, then backtracks by adding noise to a previous level and continuing the search.

Proposition 1. *In the continuous limit where the number of diffusion denoising steps $T \rightarrow \infty$, training-free guidance with recurrence is equivalent to running Langevin MCMC on a series of annealed distributions $\{\tilde{q}_t(\mathbf{x}_t)\}_{t=0}^T$, with $\tilde{q}_0(\mathbf{x}_0) = \tilde{p}_0(\mathbf{x}_0) \propto p_0(\mathbf{x}_0)f(\mathbf{x}_0)^\lambda$.*

Thus, the recurrence step (without guidance) can be interpreted as Langevin MCMC applied to the original distribution of the diffusion model $q_t(\mathbf{x}_t)$, effectively guiding the samples back toward the data manifold (details see Appendix. C.4). The guidance term then serves as defining a practical annealing path $\hat{f}_t(\mathbf{x}_t)$, biasing the sampling path. We are the *first* to propose this theoretical unification of the two lines of work, providing insights into efficient local search of diffusion models via gradients.

To implement local search, we parameterize the reverse transition kernel $\tilde{p}_\theta(\mathbf{x}_{t-1}|\mathbf{x}_t)$ as a sequence of Langevin MCMC steps in Eq. 2, followed by a denoising step with DDIM (Eq. 10) or DDPM (Eq. 11). Owing to the equivalence between Langevin MCMC and training-free guidance, we can efficiently tune hyper-parameters using the unified design space of [94], with details in Appendix. C.5. We scale up the number of local search steps and observe significant improvements across multiple tasks (Fig. 3d), highlighting the effectiveness of local search.

4.2 Global Search for Mode Identification

Although Langevin MCMC is asymptotically exact, it often struggles to transition between distant modes [36] due to its inherently local nature. This limitation is especially pronounced in the context of the multimodal distributions induced by diffusion models. To mitigate this, we propose identifying high-score modes via a global search strategy.

We model the Markov chain of the denoising process as a *fixed-depth tree*, where the transition kernel is given by $\tilde{p}_\theta(\mathbf{x}_{t-1}|\mathbf{x}_t)$. As discussed earlier, when applying local search, we parameterize the transition kernel with multiple Langevin MCMC steps, and otherwise we directly adopt conventional diffusion samplers [65, 26, 45]. Hence, our perspective unifies both stochastic and deterministic sampling with guided sampling. This abstraction decouples the transition kernel from the sampling process, enabling the application of classic tree search heuristics to develop compute-efficient exploration methods.

BFS-style linear search. Inspired by breadth-first search (BFS), which expands nodes level-by-level, we denoise a set of particles in parallel at each noise level. The simplest approach is best-of-N

sampling: generate N candidate trajectories and select the one with the highest verifier score at the final step. While simple, this strategy ignores information from intermediate stages.

To improve efficiency, similar to best-first search [56], we evaluate each intermediate particle $\{\mathbf{x}_t^k\}_{k=1}^{K_t}$ using its verifier score $f(\mathbf{x}_{0|t}^k)$, where K_t is the number of particles at timestep t . Based on these scores, we dynamically reallocate computation by sampling more children for high-scoring nodes via the reverse transition kernel $\tilde{p}_\theta(\mathbf{x}_{t-1}|\mathbf{x}_t)$. This forms the basis of *BFS-Resampling*, where each node samples children in proportion to its normalized verifier score

$$n_t^k = \text{Round} \left(K_t \frac{f(\mathbf{x}_{0|t}^k)^{\tau_t}}{\sum_{i=1}^{K_t} f(\mathbf{x}_{0|t}^i)^{\tau_t}} \right).$$

We then sample n_t^k children from \mathbf{x}_t^k using $\tilde{p}_\theta(\mathbf{x}_{t-1}|\mathbf{x}_t)$ and proceed to the next denoising step.

When using deterministic ODE solvers [45] as transition kernels, it is ineffective to sample multiple children from the same parent. To address this, we propose *BFS-Pruning*, a variant that retains only top-scoring nodes and allows at most one child per parent $n_t^k = \min(1, n_t^k)$. This leads to a gradual narrowing of the search tree as K_t decreases over time, enabling us to explore more diverse modes with more initial particles under the same compute.

As shown in Fig. 5, both resampling and pruning significantly improve efficiency over standard best-of- N sampling. The detailed pseudo code is in Alg. 3.

DFS-style non-linear search. Depth-first search (DFS) explores one branch of the search tree as deeply as possible before backtracking. In our setting, this corresponds to iteratively denoising a single particle until its verifier score drops below a predefined threshold: $f(\mathbf{x}_{0|t}) \leq \delta_t$, where δ_t is a scheduled threshold for timestep t .

Once the constraint is violated, the algorithm backtracks by reintroducing noise, moving to a higher noise level $t_{\text{next}} = t + \Delta_T$ using the forward diffusion process $q(\mathbf{x}_{t_{\text{next}}}|\mathbf{x}_t)$ in Eq. 1. This allows the model to restart the denoising process from a different region of the manifold, encouraging exploration of diverse modes. By placing a cap on the number of backtracking steps, we can explore the space globally while keeping computation bounded.

A key strength of DFS is its ability to allocate compute adaptively: difficult prompts and low-quality trajectories naturally trigger more backtracking and exploration, while easier instances are solved more directly. This dynamic behavior is driven purely by the verifier signal, without needing to know the difficulty in advance. As shown in Fig. 4, this strategy leads to substantial gains in efficiency and performance. The detailed pseudo code is in Alg. 4.

5 Experiments

In this section, we apply inference-time scaling with our search strategy across a range of domains. In Sec. 5.1, we show that diffusion models can generate long-horizon plans in complex maze environments with inference-time scaling, given a world model as verifier. In Sec. 5.2, we leverage a pretrained Q-function as a verifier to guide diffusion policies, achieving strong performance on D4RL [19] locomotion benchmarks. Finally, in Sec. 5.3, we approach the image generation task, and demonstrate that our global search algorithms consistently outperform best-of- N sampling in terms of efficiency, and we reveal interesting properties of BFS and DFS.

5.1 Long Horizon Planning

Diffusion models have been widely adopted in planning for trajectory synthesis [75]. We evaluate long-horizon planning in the PointMaze environment from OGBench [55], training the diffusion model following the approach in Diffuser [31], where the full trajectory is denoised:

$$\tau = \begin{bmatrix} \mathbf{s}_1 & \mathbf{s}_2 & \cdots & \mathbf{s}_H \\ \mathbf{a}_1 & \mathbf{a}_2 & \cdots & \mathbf{a}_H \end{bmatrix}.$$

To highlight the effectiveness of inference-time scaling, we evaluate on the largest PointMaze Giant environment and introduce an even more challenging variant, PointMaze Ultra, following the protocol from [49]. The maze layouts are shown in Fig. 3a. We define the verifier loss for each colliding point

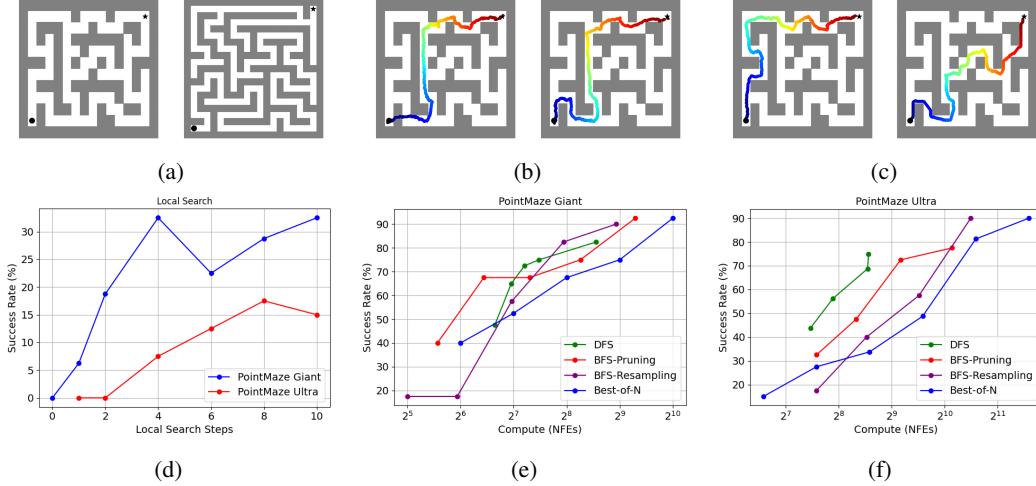


Figure 3: **(Illustration and results for maze planning)** Fig. 3a shows the maze layout of Giant (left) and Ultra (right), with start: \bullet and goal: \star . Fig. 3b illustrates the effect of local search, where left shows the directly sampled trajectory that violates the maze block on the bottom left, and right shows the successful sample after local search. Fig. 3c shows that inference time search generates diverse solutions. Fig. 3d shows the performance with scaling number of local search steps with Langevin MCMC. Fig. 3e and Fig. 3f shows the scaling behaviors of the global search methods for PointMaze Giant and PointMaze Ultra respectively. Details see Appendix. E.1.

of the trajectory as the squared distance to its nearest wall, thus the overall verifier score measures the degree the trajectory violates the environment (details see Appendix. E.1). This verifier functions as a physics-grounded instance of a *world model*. Importantly, naively maximizing the verifier score does not guarantee a successful plan, and planning remains difficult even with full access to the maze layout [46, 49].

In the most challenging scenario—navigating from the bottom-left to the top-right corner—naive sampling strategies rarely succeed, necessitating multiple local search steps (Fig. 3d). As illustrated in Fig. 3b, local search guided by the verifier enables the model to find successful plans that navigate around obstacles. As shown in Fig. 3e and Fig. 3f, incorporating global search alongside local refinement leads to over 90% success rates in both maze environments, with both BFS and DFS significantly improving search efficiency compared to naive best-of- N sampling. Moreover, as shown in Fig. 3c, global search enables the generation of diverse, high-quality solutions.

5.2 Offline Reinforcement Learning

Table 1: Performance on D4RL locomotion tasks, score normalized as suggested in [19]. Following [44] we report the mean and standard deviation over 5 independent trials, highlighting the numbers within 5 percent of the maximum in every individual task. To faithfully report our performance, we conduct the hyper-parameter search and evaluation with different seeds. For more details see Appendix. E.2.

Dataset	Environment	CQL	BCQ	IQL	SfBC	DD	Diffuser	D-QL	QGPO	TTS(ours)
Medium-Expert	HalfCheetah	62.4	64.7	86.7	92.6	90.6	79.8	96.1	93.5	93.9 ± 0.3
Medium-Expert	Hopper	98.7	100.9	91.5	108.6	111.8	107.2	110.7	108.0	104.4 ± 3.1
Medium-Expert	Walker2d	111.0	57.5	109.6	109.8	108.8	108.4	109.7	110.7	111.4 ± 0.1
Medium	HalfCheetah	44.4	40.7	47.4	45.9	49.1	44.2	50.6	54.1	54.8 ± 0.1
Medium	Hopper	58.0	54.5	66.3	57.1	79.3	58.5	82.4	98.0	99.5 ± 1.7
Medium	Walker2d	79.2	53.1	78.3	77.9	82.5	79.7	85.1	86.0	86.5 ± 0.2
Medium-Replay	HalfCheetah	46.2	38.2	44.2	37.1	39.3	42.2	47.5	47.6	47.8 ± 0.4
Medium-Replay	Hopper	48.6	33.1	94.7	86.2	100.0	96.8	100.7	96.9	97.4 ± 4.0
Medium-Replay	Walker2d	26.7	15.0	73.9	65.1	75.0	61.2	94.3	84.4	79.3 ± 9.7
Average (Locomotion)		63.9	51.9	76.9	75.6	81.8	75.3	86.3	86.6	86.1

Recently, diffusion models emerged as a powerful action prior in robotics due to its ability to model complex and multimodal distributions [10, 43]. However, these diffusion policies are typically trained on offline datasets and struggle to adapt to reinforcement learning or test-time requirements. Following prior work [57], we formulate the offline RL problem as sampling from a Q-regularized distribution:

$$\pi^*(a|s) \propto \mu(a|s)e^{\beta Q_\psi(s,a)},$$

where Q_ψ is a learned Q-function representing preferences over actions, and μ is the behavior policy, which we model using a diffusion prior.

In principle, exact sampling from π^* using diffusion models requires training a noise-dependent energy function on noisy actions a_t [31, 44]. However, this approach is often impractical in real-world settings. First, it requires evaluating the pretrained Q-function on samples from the diffusion model, which is costly due to the difficulty of data collection in robotics. Second, many Q-functions rely on foundation models as backbones [7, 51], and training them on noisy samples risks degrading their pre-trained knowledge. In contrast, *test-time search* (TTS) offers a promising alternative. By decoupling policy and value, TTS enables flexible composition with foundation models without retraining.

We evaluate TTS using both local and global search strategies on the D4RL locomotion benchmarks [19]. Following the setup in [44], we adopt their pretrained diffusion policy and ground-truth Q-function. Results are presented in Table 1, where our approach achieves performance competitive with the best training-based methods, including QGPO [44] and Diffusion-QL [80]. In comparison, our approach is *training-free*, requiring only an off the shelf Q function and diffusion model.

5.3 Image Generation

In this section we evaluate inference-time scaling in image generation tasks, especially the efficiency of global search.

5.3.1 Compositional Text-to-Image Generation

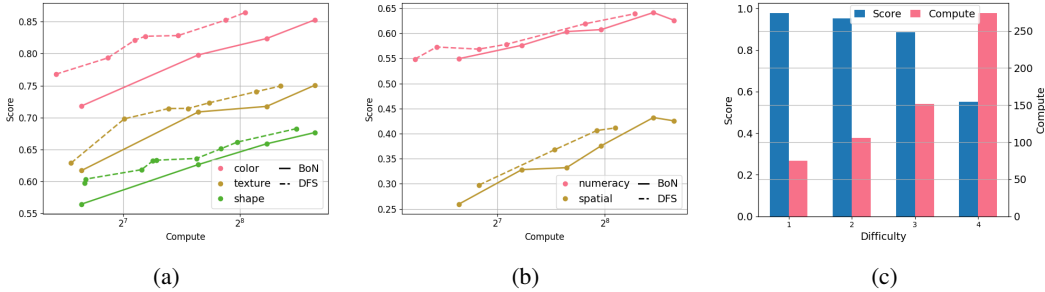


Figure 4: **CompBench [29] text-to-image results.** Fig. 4a and Fig. 4b show DFS performance on attribute binding and object relationship tasks, achieving up to 2× lower computational cost than Best-of-N. Fig. 4c presents the average compute allocated by DFS for prompts of increasing difficulty, evaluated on the color dataset.

We evaluate inference-time scaling for text-to-image generation on the CompBench dataset [29] using the SSD-1B model [22]. For the search verifiers, we use task-specific oracle verifiers: a BLIP-VQA model [37] for the attribute binding task and a UniDet model [100] for the object relationship task. Since these verifiers are non-differentiable, we apply global search exclusively. Detailed setup is in Appendix. E.3.1.

Improved efficiency and adaptivity with DFS. We evaluate Best-of-N and DFS on the five datasets in attribute binding and object relationship tasks, with each dataset consists of 300 prompts. The results are shown in Fig. 4a and Fig. 4b, where DFS consistently outperforms Best-of-N while using up to 2× less compute. To evaluate DFS’s ability to adaptively allocate computation, we divide the 300 prompts in the color dataset into four difficulty bins based on their average score over 8 samples. Using the same set of hyperparameters across all prompts, Fig. 4c shows that DFS allocates less compute to easier prompts (bin 1) and progressively more to harder ones with lower scores—demonstrating automatic, difficulty-aware compute allocation. Unlike [64], which manually selects different search strategies based on predefined difficulty labels, our method requires no prior

knowledge of difficulty. DFS dynamically adjusts compute allocation during inference using a single, unified algorithm and fixed parameters.

5.3.2 Conditional ImageNet Generation

Conditional generation of diffusion models using a unconditional foundation model has important applications [94] as foundation models obtain increasing expressivity. However, classifier guidance [12] requires training a noise-dependent classifier on samples generated by the diffusion model, which is difficult since it may require a lot of attempts for an unconditional model to generate the correct class. In this section, we treat the pretrained classifier as the verifier function and conduct inference-time scaling with both local and global search. The experimental details are in Appendix. E.3.2.

Mitigating verifier hacking with double-verifier. One of the major challenges of guiding the samples using the verifier gradient is that image classifiers are prone to adversarial examples [70]. Inspired by the double-Q learning in RL [76], we use two verifiers for local search gradient computation and global search respectively. Specifically, we use two different vision transformers [89] with input resolution 224 and 384. For accuracy evaluation we use another classifier from [74]. As shown in Table. 2, using double-verifier consistently improves performance with Best-of-N sampling, with up to 2x less compute.

Table 2: Best-of-N results for ImageNet conditional generation, with FID and Accuracy averaged across the two labels.

#Particles	Single verifier		Double-verifier	
	FID↓	Acc↑	FID↓	Acc↑
2	188.5	25.6%	178.4	29.7%
4	171.5	31.8%	151.2	37.5%
8	155.7	35.8%	127.8	49.2%

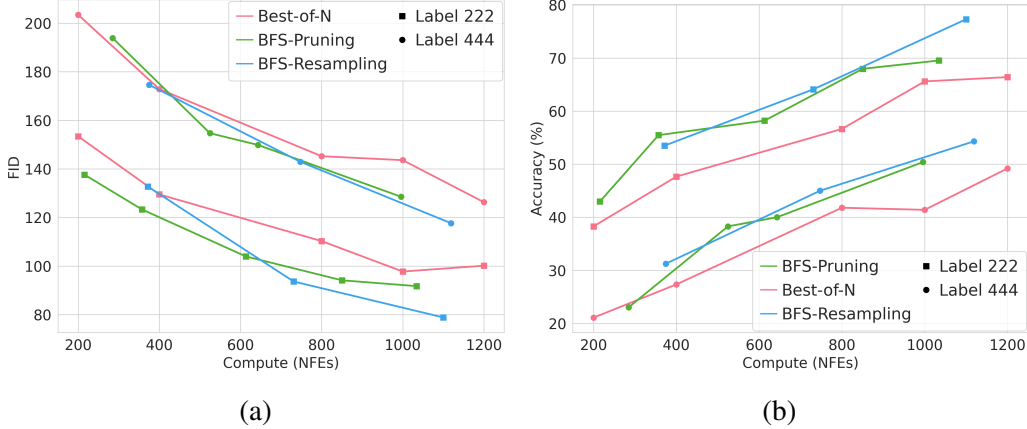


Figure 5: **Results for ImageNet conditional generation with BFS** Fig. 5a and Fig. 5b show the FID and class accuracy of conditional samples. BFS consistently outperform Best-of-N sampling in efficiency.

Improved Efficiency with BFS. We investigate breadth-first search (BFS) as a means to improve the computational efficiency of Best-of-N sampling. All experiments use the double-verifier setup, where one verifier guides gradient-based local search and the other handles resampling or pruning. As shown in Fig. 5, both BFS-Resampling and BFS-Pruning outperform Best-of-N in terms of compute efficiency. BFS-Pruning is more effective under limited compute budgets, while BFS-Resampling achieves higher performance with increased compute.

6 Limitations and Conclusion

Limitations. Despite the performance improvement of inference-time scaling, it still requires more hyperparameter tuning than training-based methods. One approach is to design an adaptive hyperparameter tuning framework, which could increase or decrease automatically based on the current sample. For example we can tune the threshold of DFS automatically given the pass rate of samples. Another potential concern is that the generated samples may be used as adversarial examples to attack verifiers. Our method can be used to search for weaknesses of verifiers, which in turn can be used to train a more robust verifier.

Conclusion. In this work we propose a principled framework for inference-time scaling through classic search principles, unlocking the potential of scaling inference-time compute of diffusion models in a variety of downstream tasks. Inference-scaling can also be applied to training models via expert iteration, generating high-quality synthetic data beyond the model’s ability. We leave this as an interesting future direction.

References

- [1] A. Ajay, Y. Du, A. Gupta, J. Tenenbaum, T. Jaakkola, and P. Agrawal. Is conditional generative modeling all you need for decision-making? *arXiv preprint arXiv:2211.15657*, 2022. 24
- [2] M. S. Albergo and E. Vanden-Eijnden. Building normalizing flows with stochastic interpolants. *arXiv preprint arXiv:2209.15571*, 2022. 3
- [3] T. Anthony, Z. Tian, and D. Barber. Thinking Fast and Slow with Deep Learning and Tree Search, Dec. 2017. arXiv:1705.08439 [cs]. 2
- [4] A. Bansal, H.-M. Chu, A. Schwarzschild, S. Sengupta, M. Goldblum, J. Geiping, and T. Goldstein. Universal guidance for diffusion models. In *Proceedings of the IEEE/CVF Conference on Computer Vision and Pattern Recognition*, pages 843–852, 2023. 16
- [5] K. Black, N. Brown, D. Driess, A. Esmail, M. Equi, C. Finn, N. Fusai, L. Groom, K. Hausman, B. Ichter, et al. π_0 : A vision-language-action flow model for general robot control. *arXiv preprint arXiv:2410.24164*, 2024. 1, 16
- [6] K. Black, M. Janner, Y. Du, I. Kostrikov, and S. Levine. Training diffusion models with reinforcement learning. *arXiv preprint arXiv:2305.13301*, 2023. 16
- [7] A. Brohan, Y. Chebotar, C. Finn, K. Hausman, A. Herzog, D. Ho, J. Ibarz, A. Irpan, E. Jang, R. Julian, et al. Do as i can, not as i say: Grounding language in robotic affordances. In *Conference on robot learning*, pages 287–318. PMLR, 2023. 8
- [8] H. Chen, C. Lu, C. Ying, H. Su, and J. Zhu. Offline reinforcement learning via high-fidelity generative behavior modeling. In *The Eleventh International Conference on Learning Representations*, 2023. 24
- [9] X. Cheng and P. Bartlett. Convergence of langevin mcmc in kl-divergence. In *Algorithmic learning theory*, pages 186–211. PMLR, 2018. 17
- [10] C. Chi, Z. Xu, S. Feng, E. Cousineau, Y. Du, B. Burchfiel, R. Tedrake, and S. Song. Diffusion policy: Visuomotor policy learning via action diffusion. *The International Journal of Robotics Research*, page 02783649241273668, 2023. 1, 8, 16
- [11] H. Chung and J. C. Ye. Score-based diffusion models for accelerated mri. *Medical image analysis*, 80:102479, 2022. 16
- [12] P. Dhariwal and A. Nichol. Diffusion models beat gans on image synthesis. *Advances in neural information processing systems*, 34:8780–8794, 2021. 1, 3, 9, 16, 25
- [13] K. Dong and T. Ma. STP: Self-play LLM Theorem Provers with Iterative Conjecturing and Proving, Mar. 2025. arXiv:2502.00212 [cs]. 16
- [14] Y. Du, C. Durkan, R. Strudel, J. B. Tenenbaum, S. Dieleman, R. Fergus, J. Sohl-Dickstein, A. Doucet, and W. S. Grathwohl. Reduce, reuse, recycle: Compositional generation with energy-based diffusion models and mcmc. In *International conference on machine learning*, pages 8489–8510. PMLR, 2023. 3, 4, 16, 17
- [15] Y. Du, J. Mao, and J. B. Tenenbaum. Learning Iterative Reasoning through Energy Diffusion, June 2024. arXiv:2406.11179 [cs]. 3
- [16] Y. Du and I. Mordatch. Implicit generation and modeling with energy based models. *Advances in neural information processing systems*, 32, 2019. 17

- [17] A. Durmus and E. Moulines. Non-asymptotic convergence analysis for the unadjusted langevin algorithm. *arXiv preprint arXiv:1507.05021*, 2015. 17
- [18] P. Esser, S. Kulal, A. Blattmann, R. Entezari, J. Müller, H. Saini, Y. Levi, D. Lorenz, A. Sauer, F. Boesel, et al. Scaling rectified flow transformers for high-resolution image synthesis. In *Forty-first international conference on machine learning*, 2024. 16
- [19] J. Fu, A. Kumar, O. Nachum, G. Tucker, and S. Levine. D4rl: Datasets for deep data-driven reinforcement learning. *arXiv preprint arXiv:2004.07219*, 2020. 6, 7, 8
- [20] S. Fujimoto, D. Meger, and D. Precup. Off-policy deep reinforcement learning without exploration. In *International conference on machine learning*, pages 2052–2062. PMLR, 2019. 24
- [21] D. Guo, D. Yang, H. Zhang, J. Song, R. Zhang, R. Xu, Q. Zhu, S. Ma, P. Wang, X. Bi, et al. Deepseek-r1: Incentivizing reasoning capability in llms via reinforcement learning. *arXiv preprint arXiv:2501.12948*, 2025. 15
- [22] Y. Gupta, V. V. Jaddipal, H. Prabhala, S. Paul, and P. Von Platen. Progressive knowledge distillation of stable diffusion xl using layer level loss. *arXiv preprint arXiv:2401.02677*, 2024. 8
- [23] X. Han, S. Kumar, and Y. Tsvetkov. Ssd-lm: Semi-autoregressive simplex-based diffusion language model for text generation and modular control. *arXiv preprint arXiv:2210.17432*, 2022. 16
- [24] P. E. Hart, N. J. Nilsson, and B. Raphael. A formal basis for the heuristic determination of minimum cost paths. *IEEE transactions on Systems Science and Cybernetics*, 4(2):100–107, 1968. 1
- [25] Y. He, N. Murata, C.-H. Lai, Y. Takida, T. Uesaka, D. Kim, W.-H. Liao, Y. Mitsufuji, J. Z. Kolter, R. Salakhutdinov, et al. Manifold preserving guided diffusion. *arXiv preprint arXiv:2311.16424*, 2023. 16
- [26] J. Ho, A. Jain, and P. Abbeel. Denoising diffusion probabilistic models. *Advances in neural information processing systems*, 33:6840–6851, 2020. 1, 3, 5, 16, 19
- [27] J. Ho and T. Salimans. Classifier-free diffusion guidance. *arXiv preprint arXiv:2207.12598*, 2022. 24
- [28] J. Ho, T. Salimans, A. Gritsenko, W. Chan, M. Norouzi, and D. J. Fleet. Video diffusion models. *Advances in Neural Information Processing Systems*, 35:8633–8646, 2022. 1, 16
- [29] K. Huang, K. Sun, E. Xie, Z. Li, and X. Liu. T2i-compbench: A comprehensive benchmark for open-world compositional text-to-image generation. *Advances in Neural Information Processing Systems*, 36:78723–78747, 2023. 1, 8, 24
- [30] A. Jaech, A. Kalai, A. Lerer, A. Richardson, A. El-Kishky, A. Low, A. Helyar, A. Madry, A. Beutel, A. Carney, et al. Openai o1 system card. *arXiv preprint arXiv:2412.16720*, 2024. 3, 15
- [31] M. Janner, Y. Du, J. Tenenbaum, and S. Levine. Planning with diffusion for flexible behavior synthesis. In *International Conference on Machine Learning*, pages 9902–9915. PMLR, 2022. 6, 8, 16, 23, 24
- [32] D. Kahneman. *Thinking, fast and slow*. macmillan, 2011. 2, 15, 16
- [33] S. Kirkpatrick, C. D. Gelatt Jr, and M. P. Vecchi. Optimization by simulated annealing. *science*, 220(4598):671–680, 1983. 17
- [34] I. Kostrikov, A. Nair, and S. Levine. Offline reinforcement learning with implicit q-learning. *arXiv preprint arXiv:2110.06169*, 2021. 24
- [35] A. Kumar, A. Zhou, G. Tucker, and S. Levine. Conservative q-learning for offline reinforcement learning. *Advances in neural information processing systems*, 33:1179–1191, 2020. 24

- [36] K. Łatuszyński, M. T. Moores, and T. Stumpf-Fétizon. Mcmc for multi-modal distributions. *arXiv preprint arXiv:2501.05908*, 2025. 5
- [37] J. Li, D. Li, C. Xiong, and S. Hoi. Blip: Bootstrapping language-image pre-training for unified vision-language understanding and generation. In *International conference on machine learning*, pages 12888–12900. PMLR, 2022. 8
- [38] S. Li, K. Kallidromitis, A. Gokul, A. Koneru, Y. Kato, K. Kozuka, and A. Grover. Reflect-dit: Inference-time scaling for text-to-image diffusion transformers via in-context reflection. *arXiv preprint arXiv:2503.12271*, 2025. 16
- [39] H. Lightman, V. Kosaraju, Y. Burda, H. Edwards, B. Baker, T. Lee, J. Leike, J. Schulman, I. Sutskever, and K. Cobbe. Let’s verify step by step. In *The Twelfth International Conference on Learning Representations*, 2023. 3, 15
- [40] S. Lin, B. Liu, J. Li, and X. Yang. Common diffusion noise schedules and sample steps are flawed. In *Proceedings of the IEEE/CVF winter conference on applications of computer vision*, pages 5404–5411, 2024. 21
- [41] Y. Lipman, R. T. Chen, H. Ben-Hamu, M. Nickel, and M. Le. Flow matching for generative modeling. *arXiv preprint arXiv:2210.02747*, 2022. 3
- [42] N. Liu, S. Li, Y. Du, A. Torralba, and J. B. Tenenbaum. Compositional visual generation with composable diffusion models. In *European Conference on Computer Vision*, pages 423–439. Springer, 2022. 16
- [43] S. Liu, L. Wu, B. Li, H. Tan, H. Chen, Z. Wang, K. Xu, H. Su, and J. Zhu. Rdt-1b: a diffusion foundation model for bimanual manipulation. *arXiv preprint arXiv:2410.07864*, 2024. 1, 8, 16, 24
- [44] C. Lu, H. Chen, J. Chen, H. Su, C. Li, and J. Zhu. Contrastive energy prediction for exact energy-guided diffusion sampling in offline reinforcement learning. In *International Conference on Machine Learning*, pages 22825–22855. PMLR, 2023. 1, 3, 7, 8, 24
- [45] C. Lu, Y. Zhou, F. Bao, J. Chen, C. Li, and J. Zhu. Dpm-solver: A fast ode solver for diffusion probabilistic model sampling in around 10 steps. *Advances in Neural Information Processing Systems*, 35:5775–5787, 2022. 5, 6
- [46] Y. Luo, C. Sun, J. B. Tenenbaum, and Y. Du. Potential based diffusion motion planning. *arXiv preprint arXiv:2407.06169*, 2024. 7
- [47] N. Ma, M. Goldstein, M. S. Albergo, N. M. Boffi, E. Vanden-Eijnden, and S. Xie. Sit: Exploring flow and diffusion-based generative models with scalable interpolant transformers. In *European Conference on Computer Vision*, pages 23–40. Springer, 2024. 3, 18
- [48] N. Ma, S. Tong, H. Jia, H. Hu, Y.-C. Su, M. Zhang, X. Yang, Y. Li, T. Jaakkola, X. Jia, et al. Inference-time scaling for diffusion models beyond scaling denoising steps. *arXiv preprint arXiv:2501.09732*, 2025. 2, 3, 16
- [49] T. Marcucci, M. Petersen, D. von Wrangel, and R. Tedrake. Motion planning around obstacles with convex optimization. *Science robotics*, 8(84):eadf7843, 2023. 6, 7, 23
- [50] E. F. Moore. The shortest path through a maze. In *Proc. of the International Symposium on the Theory of Switching*, pages 285–292. Harvard University Press, 1959. 1
- [51] M. Nakamoto, O. Mees, A. Kumar, and S. Levine. Steering your generalists: Improving robotic foundation models via value guidance. In *8th Annual Conference on Robot Learning*, 2024. 3, 8
- [52] A. Newell, J. C. Shaw, and H. A. Simon. Report on a general problem solving program. In *IFIP congress*, volume 256, page 64. Pittsburgh, PA, 1959. 2, 15
- [53] A. Newell, H. A. Simon, et al. *Human problem solving*, volume 104. Prentice-hall Englewood Cliffs, NJ, 1972. 2, 15

- [54] A. Q. Nichol and P. Dhariwal. Improved denoising diffusion probabilistic models. In *International conference on machine learning*, pages 8162–8171. PMLR, 2021. 3, 19
- [55] S. Park, K. Frans, B. Eysenbach, and S. Levine. Ogbench: Benchmarking offline goal-conditioned rl. *arXiv preprint arXiv:2410.20092*, 2024. 6, 23
- [56] J. Pearl. *Heuristics: intelligent search strategies for computer problem solving*. Addison-Wesley Longman Publishing Co., Inc., 1984. 1, 6
- [57] J. Peters, K. Mulling, and Y. Altun. Relative entropy policy search. In *Proceedings of the AAAI Conference on Artificial Intelligence*, volume 24, pages 1607–1612, 2010. 8
- [58] S. Russell and P. Norvig. *Artificial Intelligence: A Modern Approach*. Prentice Hall Press, USA, 3rd edition, 2009. 1
- [59] S. Sahoo, M. Arriola, Y. Schiff, A. Gokaslan, E. Marroquin, J. Chiu, A. Rush, and V. Kuleshov. Simple and effective masked diffusion language models. *Advances in Neural Information Processing Systems*, 37:130136–130184, 2024. 16
- [60] Y. Shen, X. Jiang, Y. Yang, Y. Wang, D. Han, and D. Li. Understanding and improving training-free loss-based diffusion guidance. *Advances in Neural Information Processing Systems*, 37:108974–109002, 2024. 4
- [61] A. Singh, J. D. Co-Reyes, R. Agarwal, A. Anand, P. Patil, X. Garcia, P. J. Liu, J. Harrison, J. Lee, K. Xu, et al. Beyond human data: Scaling self-training for problem-solving with language models. *arXiv preprint arXiv:2312.06585*, 2023. 16
- [62] R. Singhal, Z. Horvitz, R. Teehan, M. Ren, Z. Yu, K. McKeown, and R. Ranganath. A general framework for inference-time scaling and steering of diffusion models. *arXiv preprint arXiv:2501.06848*, 2025. 16
- [63] S. A. Sloman. The empirical case for two systems of reasoning. *Psychological bulletin*, 119(1):3, 1996. 15
- [64] C. Snell, J. Lee, K. Xu, and A. Kumar. Scaling llm test-time compute optimally can be more effective than scaling model parameters. *arXiv preprint arXiv:2408.03314*, 2024. 3, 8, 15
- [65] J. Song, C. Meng, and S. Ermon. Denoising diffusion implicit models. *arXiv preprint arXiv:2010.02502*, 2020. 3, 5, 18
- [66] J. Song, Q. Zhang, H. Yin, M. Mardani, M.-Y. Liu, J. Kautz, Y. Chen, and A. Vahdat. Loss-guided diffusion models for plug-and-play controllable generation. In *International Conference on Machine Learning*, pages 32483–32498. PMLR, 2023. 1, 16
- [67] Y. Song and S. Ermon. Generative Modeling by Estimating Gradients of the Data Distribution, Oct. 2020. *arXiv:1907.05600*. 17
- [68] Y. Song, J. Sohl-Dickstein, D. P. Kingma, A. Kumar, S. Ermon, and B. Poole. Score-based generative modeling through stochastic differential equations. *arXiv preprint arXiv:2011.13456*, 2020. 16
- [69] V. Subramaniam, Y. Du, J. B. Tenenbaum, A. Torralba, S. Li, and I. Mordatch. Multiagent finetuning: Self improvement with diverse reasoning chains. *arXiv preprint arXiv:2501.05707*, 2025. 16
- [70] C. Szegedy, W. Zaremba, I. Sutskever, J. Bruna, D. Erhan, I. Goodfellow, and R. Fergus. Intriguing properties of neural networks. *arXiv preprint arXiv:1312.6199*, 2013. 9
- [71] Z. Tan, S. Liu, X. Yang, Q. Xue, and X. Wang. Ominicontrol: Minimal and universal control for diffusion transformer. *arXiv preprint arXiv:2411.15098*, 2024. 16
- [72] R. Tarjan. Depth-first search and linear graph algorithms. *SIAM journal on computing*, 1(2):146–160, 1972. 1

- [73] O. M. Team, D. Ghosh, H. Walke, K. Pertsch, K. Black, O. Mees, S. Dasari, J. Hejna, T. Kreiman, C. Xu, et al. Octo: An open-source generalist robot policy. *arXiv preprint arXiv:2405.12213*, 2024. [1](#), [16](#)
- [74] H. Touvron, M. Cord, M. Douze, F. Massa, A. Sablayrolles, and H. Jégou. Training data-efficient image transformers & distillation through attention. In *International conference on machine learning*, pages 10347–10357. PMLR, 2021. [9](#)
- [75] T. Ubukata, J. Li, and K. Tei. Diffusion model for planning: A systematic literature review. *arXiv preprint arXiv:2408.10266*, 2024. [6](#)
- [76] H. Van Hasselt, A. Guez, and D. Silver. Deep reinforcement learning with double q-learning. In *Proceedings of the AAAI conference on artificial intelligence*, volume 30, 2016. [3](#), [9](#), [16](#)
- [77] P. Vincent. A connection between score matching and denoising autoencoders. *Neural computation*, 23(7):1661–1674, 2011. [2](#), [3](#)
- [78] B. Wallace, M. Dang, R. Rafailov, L. Zhou, A. Lou, S. Purushwalkam, S. Ermon, C. Xiong, S. Joty, and N. Naik. Diffusion model alignment using direct preference optimization. In *Proceedings of the IEEE/CVF Conference on Computer Vision and Pattern Recognition*, pages 8228–8238, 2024. [1](#), [16](#)
- [79] G. Wang, S. Zhang, T. Zhan, Z. Shen, J. Li, X. Hu, X. Sun, F. Wu, G. Deng, J. Zhang, et al. Unlocking the mysteries of openai o1: A survey of the reasoning abilities of large language models. [16](#)
- [80] Z. Wang, J. J. Hunt, and M. Zhou. Diffusion policies as an expressive policy class for offline reinforcement learning. *arXiv preprint arXiv:2208.06193*, 2022. [8](#), [24](#)
- [81] J. Wei, X. Wang, D. Schuurmans, M. Bosma, F. Xia, E. Chi, Q. V. Le, D. Zhou, et al. Chain-of-thought prompting elicits reasoning in large language models. *Advances in neural information processing systems*, 35:24824–24837, 2022. [3](#)
- [82] M. Welling and Y. W. Teh. Bayesian learning via stochastic gradient langevin dynamics. In *Proceedings of the 28th international conference on machine learning (ICML-11)*, pages 681–688. Citeseer, 2011. [3](#)
- [83] A. Wibisono. Sampling as optimization in the space of measures: The langevin dynamics as a composite optimization problem. In *Conference on learning theory*, pages 2093–3027. PMLR, 2018. [4](#), [16](#)
- [84] L. Wu, B. Trippe, C. Naesseth, D. Blei, and J. P. Cunningham. Practical and asymptotically exact conditional sampling in diffusion models. *Advances in Neural Information Processing Systems*, 36:31372–31403, 2023. [16](#)
- [85] Y. Wu, Z. Sun, S. Li, S. Welleck, and Y. Yang. Inference scaling laws: An empirical analysis of compute-optimal inference for problem-solving with language models. *arXiv preprint arXiv:2408.00724*, 2024. [3](#), [15](#)
- [86] Z. Wu, S. Huang, Z. Zhou, H. Ying, J. Wang, D. Lin, and K. Chen. Internlm2. 5-stepprover: Advancing automated theorem proving via expert iteration on large-scale lean problems. *arXiv preprint arXiv:2410.15700*, 2024. [16](#)
- [87] E. Xie, J. Chen, Y. Zhao, J. Yu, L. Zhu, C. Wu, Y. Lin, Z. Zhang, M. Li, J. Chen, et al. Sana 1.5: Efficient scaling of training-time and inference-time compute in linear diffusion transformer. *arXiv preprint arXiv:2501.18427*, 2025. [1](#)
- [88] Y. Xie, V. Jampani, L. Zhong, D. Sun, and H. Jiang. Omnicontrol: Control any joint at any time for human motion generation. *arXiv preprint arXiv:2310.08580*, 2023. [16](#)
- [89] J. Xu, X. Liu, Y. Wu, Y. Tong, Q. Li, M. Ding, J. Tang, and Y. Dong. Imagereward: learning and evaluating human preferences for text-to-image generation. In *Proceedings of the 37th International Conference on Neural Information Processing Systems*, pages 15903–15935, 2023. [1](#), [9](#), [16](#)

- [90] M. Xu, L. Yu, Y. Song, C. Shi, S. Ermon, and J. Tang. Geodiff: A geometric diffusion model for molecular conformation generation. *arXiv preprint arXiv:2203.02923*, 2022. 16
- [91] Y. Xu, M. Deng, X. Cheng, Y. Tian, Z. Liu, and T. Jaakkola. Restart sampling for improving generative processes. *Advances in Neural Information Processing Systems*, 36:76806–76838, 2023. 16
- [92] S. Yang, Y. Du, S. K. S. Ghasemipour, J. Tompson, L. P. Kaelbling, D. Schuurmans, and P. Abbeel. Learning interactive real-world simulators. In *The Twelfth International Conference on Learning Representations*, 2024. 1
- [93] S. Yao, D. Yu, J. Zhao, I. Shafran, T. Griffiths, Y. Cao, and K. Narasimhan. Tree of thoughts: Deliberate problem solving with large language models. *Advances in neural information processing systems*, 36:11809–11822, 2023. 2, 15
- [94] H. Ye, H. Lin, J. Han, M. Xu, S. Liu, Y. Liang, J. Ma, J. Y. Zou, and S. Ermon. Tfg: Unified training-free guidance for diffusion models. *Advances in Neural Information Processing Systems*, 37:22370–22417, 2024. 1, 4, 5, 9, 16, 19, 20
- [95] J. Yu, Y. Wang, C. Zhao, B. Ghanem, and J. Zhang. Freedom: Training-free energy-guided conditional diffusion model. In *Proceedings of the IEEE/CVF International Conference on Computer Vision*, pages 23174–23184, 2023. 4, 16
- [96] E. Zelikman, Y. Wu, J. Mu, and N. Goodman. Star: Bootstrapping reasoning with reasoning. *Advances in Neural Information Processing Systems*, 35:15476–15488, 2022. 16
- [97] L. Zhang, A. Rao, and M. Agrawala. Adding conditional control to text-to-image diffusion models. In *Proceedings of the IEEE/CVF international conference on computer vision*, pages 3836–3847, 2023. 16
- [98] Y. Zhang, E. Tzeng, Y. Du, and D. Kislyuk. Large-scale reinforcement learning for diffusion models. In *European Conference on Computer Vision*, pages 1–17. Springer, 2024. 16
- [99] S. Zhao, R. Brekelmans, A. Makhzani, and R. Grosse. Probabilistic inference in language models via twisted sequential monte carlo. *arXiv preprint arXiv:2404.17546*, 2024. 16
- [100] X. Zhou, V. Koltun, and P. Krähenbühl. Simple multi-dataset detection. In *Proceedings of the IEEE/CVF conference on computer vision and pattern recognition*, pages 7571–7580, 2022. 8

A Appendix Overview

In Sec. B, we provide a in-depth review of literature related to inference-time scaling and diffusion models. In Sec. C, we elaborate on local search with Langevin MCMC, and in Sec. D we provide the pseudo code and design of global search algorithms BFS and DFS. In Sec. E, we provide the details of all the experiments.

B Additional Related Works

Inference-time scaling. Scaling compute in inference-time with “slow thinking” has its long history grounded in cognitive science, known as “system 2” thinking [32, 63]. In [52, 53], Newell and his colleagues formalized problem solving as tree search in a combinatorial space, and [93] uses tree-of-thoughts to enable LLM reasoning with multiple exploration paths, using BFS and DFS as strategic search algorithms.

Recently, long chain-of-thought (CoT) reasoning has demonstrated remarkable performance for LLM reasoning [30, 21], where the long CoT reasoning ability is incentivized through reinforcement learning [21]. Notably, the CoT process demonstrates reasoning activities such as self-verification, backtracking and self-correction. Using a process reward model [39], we can also conduct explicit tree search without training the language model. [85] propose reward-balanced search (REBASE) which is a special instance of BFS, and [64] applied beam-search to difficult math problems, showing

compute-optimal inference can be achieved via selecting different strategy for problems with different difficulty. We refer the readers to [79] for a comprehensive review.

Inference-time scaling could also be used to improve the model itself, known as expert iteration. In [32], they proposed reinforcement learning with expert iteration in games, where the expert is constructed combining the base policy with Monte Carlo Tree Search (MCTS), and [86] applied expert iteration to automated theorem proving. Self improvements can also be achieved through iterative self-training [69, 96, 13, 61].

Inference scaling in diffusion models. The inference-time compute of diffusion models depends heavily on the number of denoising steps. [91] showed that recursive restart sampling can reduce cumulative error during sampling, which can be regarded as scaling the number of denoising steps. More recently, [62] proposed a Sequential Monte Carlo (SMC) [84, 99] style method, known as Feynman-Kac steering, which can be seen as an instance of BFS. Besides image generation, they also applied it to diffusion language models [23, 59]. Additionally, [48] explored inference-time scaling of diffusion models with local zero order search and global search over paths for image generation. They also experimented with different verifiers, such as oracle verifiers, self-supervised verifiers, and studied the verifier-task alignment problem. Their zero-order search can be understood as an uninformed version of local search which exhibits low efficiency, and when utilizing gradients, they need to back-propagate through the entire diffusion sampling chain, causing high computation and memory overheads. Compared with their work, we propose efficient gradient-based local search with theoretically grounded Langevin MCMC, which we show is crucial in many tasks. Also, we provide systematic experiments on the compute efficiency of global search methods. Their proposed methods can thus be understood as an instance within our search framework.

Apart from search, [38] exploits the in-context learning abilities of foundation models to provide revision during sampling. Specifically, they leverage the multi-modal capabilities of VLMs to provide feedbacks on past generated images, and train the model to condition on past images and feedback.

Diffusion models and applications. Diffusion models [26, 68, 76] has shown great performance in generative modeling for continuous data domains, such as image [18, 12], videos [28] and molecules [90]. Due to its expressive power on modeling multimodal and complex distributions, they have also been widely used as a decision prior in robotics. [31] proposes the first work on using diffusion models to generate plans. [10] uses the diffusion model for visuo-motor policy in robotics. Recently, a series of robotics foundation models utilize diffusion heads as action experts [5, 73], while [43] trains a end-to-end diffusion transformer for bimanual manipulation. In this work, we demonstrate that inference-time scaling can be especially helpful for decision making tasks with diffusion models.

Control and alignment of diffusion models. To align the diffusion model with flexible objectives, training-free guidance [94, 4, 11, 66, 95, 25] and compositional generation [14, 42] combines the diffusion models with classifiers or other diffusion models at inference time, while RL-based methods [98, 78, 89, 6] finetune the diffusion model using reward or preference signals. ControlNet [97] style approaches have also been used to add additional conditions for sampling, where [71] designs a control block for diffusion transformers, and [88] uses a combination of guidance and controlnet for controllable human motion generation.

C Details about local search with Langevin MCMC

In this section we provide a comprehensive and detailed overview of (annealed) Langevin MCMC based methods used in local search, as well as proving Proposition. 1.

C.1 Langevin MCMC as gradient flow in measure space

Following [83], the Langevin SDE in sample space corresponds to gradient flow of the KL-divergence in measure space. Here we provide a brief overview.

Define our target distribution that we wish to sample from as ν , and the distribution of our current sample as ρ . We define the KL-divergence (relative entropy) as:

$$H_\nu(\rho) = \int \rho \log \frac{\rho}{\nu}. \quad (5)$$

Thus, sampling from ν can be seen as minimizing H , since the minimum of H is achieved at $\rho = \nu$ with $H_\nu(\rho) = 0$. Furthermore, ν is the only stationary point of H even for multimodal distributions. Thus we can sample from ν when optimizing H via gradient based methods.

We have the gradient flow of H in Eq. 5 follows the following PDE:

$$\frac{\partial \rho}{\partial t} = \nabla \cdot (\rho \nabla (-\log \nu)) + \Delta \rho, \quad (6)$$

which is known as the Fokker-Planck equation. Here, $\rho = \rho(\mathbf{x}, t)$ is a smooth positive density evolving through time, driven by the dynamics of the sample \mathbf{x} . The dynamics in sample space corresponding to Eq. 6 is the Langevin SDE:

$$d\mathbf{x}_t = \nabla \log \nu(\mathbf{x}_t) dt + \sqrt{2} d\mathbf{w}_t. \quad (7)$$

where $(\mathbf{x}_t)_{t \geq 0}$ is a stochastic process with measure ρ_t , and $(\mathbf{w}_t)_{t \geq 0}$ is standard Brownian motion. That is, if $\mathbf{x}_t \sim \rho_t$ evolves according to the dynamics in Eq. 7, then the measure $\rho(\mathbf{x}, t) = \rho_t$ evolves according to the PDE in Eq. 6, conducting gradient optimization in measure space.

In practice, we implement Eq. 7 through discretization, which is known as the unadjusted Langevin algorithm (ULA):

$$\mathbf{x}^{i+1} = \mathbf{x}^i + \eta \nabla_{\mathbf{x}^i} \log \nu(\mathbf{x}^i) + \sqrt{2\eta} \epsilon^i, \quad (8)$$

with $\epsilon^i \sim \mathcal{N}(\mathbf{0}, \mathbf{I})$. When $\eta \rightarrow 0$, the ULA converges to Langevin SDE, providing exact sampling.

Previous works [17, 9] show that ULA can efficiently converge to the target measure ν if ν is log-concave and smooth. However, when facing complex and multimodal distributions, we can only guarantee convergence to the concave vicinity.

C.2 Annealed Langevin MCMC Sampling

Langevin MCMC have been used to perform implicit sampling in energy-based models [16] and score-based models [67]. However, these methods suffer from inaccurate score estimation and low density regions [67]. In [67] they propose to perturb the data with gaussian noise, eventually smoothing the data distribution:

$$q(\mathbf{x}_t) = \int_{\mathbf{x}_0} p_0(\mathbf{x}_0) \mathcal{N}(\mathbf{x}_t; \mathbf{x}_0, \sigma_t^2 \mathbf{I}),$$

and creating a sequence of annealed distributions $\{q(\mathbf{x}_t)\}_{t=0}^T$ which converges to $p_0(\mathbf{x}_0)$. Since they are smoothed by gaussian noise, we can improve the mixing time of Langevin MCMC on multimodal distributions by sampling from these intermediate distributions, sharing similar spirits with simulated annealing [33].

In [14], they extend this method to compositional generation of diffusion models. Specifically, we consider sampling from a product distribution $p_0^{\text{prod}}(\mathbf{x}_0) \propto p_0^1(\mathbf{x}_0) p_0^2(\mathbf{x}_0)$, where $p_0^1(\mathbf{x}_0)$ and $p_0^2(\mathbf{x}_0)$ are distributions of different diffusion models. Since we have access to the score functions $\nabla_{\mathbf{x}_t} \log q_t^1(\mathbf{x}_t)$ and $\nabla_{\mathbf{x}_t} \log q_t^2(\mathbf{x}_t)$ through the diffusion model, we can construct a sequence of annealing distributions $\tilde{q}_t^{\text{prod}}(\mathbf{x}_t)$ such that:

$$\nabla_{\mathbf{x}_t} \log \tilde{q}_t^{\text{prod}}(\mathbf{x}_t) = \nabla_{\mathbf{x}_t} \log q_t^1(\mathbf{x}_t) + \nabla_{\mathbf{x}_t} \log q_t^2(\mathbf{x}_t).$$

By sampling from the sequence $\{\tilde{q}_t^{\text{prod}}(\mathbf{x}_t)\}$, we can arrive at $\tilde{q}_0^{\text{prod}}(\mathbf{x}_0)$ which is equal to $p_0^{\text{prod}}(\mathbf{x}_0)$.

A key difference from sampling from $\{\tilde{q}_t^{\text{prod}}(\mathbf{x}_t)\}$ and direct diffusion sampling is that the diffusion process with $p_0^{\text{prod}}(\mathbf{x}_0)$ defined as

$$q_t^{\text{prod}}(\mathbf{x}_t) = \int_{\mathbf{x}_0} p_0^{\text{prod}}(\mathbf{x}_0) q(\mathbf{x}_t | \mathbf{x}_0)$$

is different from $\tilde{q}_t^{\text{prod}}(\mathbf{x}_t)$. The score of $q_t^{\text{prod}}(\mathbf{x}_t)$ can be derived as:

$$\nabla_{\mathbf{x}_t} \log q_t^{\text{prod}}(\mathbf{x}_t) = \nabla_{\mathbf{x}_t} \log \left(\int_{\mathbf{x}_0} p_0^1(\mathbf{x}_0) p_0^2(\mathbf{x}_0) q(\mathbf{x}_t | \mathbf{x}_0) \right),$$

which is not equal to

$$\nabla_{\mathbf{x}_t} \log \tilde{q}_t^{\text{prod}}(\mathbf{x}_t) = \nabla_{\mathbf{x}_t} \log \left(\int_{\mathbf{x}_0} p_0^1(\mathbf{x}_0) q(\mathbf{x}_t | \mathbf{x}_0) \right) + \nabla_{\mathbf{x}_t} \log \left(\int_{\mathbf{x}_0} p_0^2(\mathbf{x}_0) q(\mathbf{x}_t | \mathbf{x}_0) \right),$$

and thus intractable to compute directly.

A key distinction between annealed Langevin MCMC sampling and reverse diffusion sampling is that we run multiple Langevin MCMC steps on the *same noise level*, while reverse diffusion goes from high noise level to low noise level via denoising. A minimal pseudo code is shown in Alg. 1.

Algorithm 1 Annealed Langevin MCMC sampling

Input: sequence of annealing distributions $\{\tilde{q}_t(\mathbf{x}_t)\}_{t=0}^T$, number of MCMC steps N , step size $\{\eta_t\}_{t=0}^T$. (Optional) reverse transition kernel $\{\tilde{p}_\theta(\mathbf{x}_{t-1} | \mathbf{x}_t)\}_{t=0}^T$.

Init: $\mathbf{x}_T^0 \sim \mathcal{N}(\mathbf{0}, \mathbf{I})$

for $t = T, \dots, 1$ **do**

for $i = 0, 1, \dots, N - 1$ **do**

 Perform Langevin MCMC steps:

$$\mathbf{x}_t^{i+1} = \mathbf{x}_t^i + \eta_t \nabla_{\mathbf{x}_t} \log \tilde{q}_t(\mathbf{x}_t^i) + \sqrt{2\eta_t} \boldsymbol{\epsilon}_t^i, \quad \boldsymbol{\epsilon}_t^i \sim \mathcal{N}(\mathbf{0}, \mathbf{I}).$$

end for

 (Optional) transit to next time step: $\mathbf{x}_{t-1}^0 \sim \tilde{p}_\theta(\cdot | \mathbf{x}_t^N)$. If no reverse kernel initialize $\mathbf{x}_{t-1}^0 = \mathbf{x}_t^N$.

end for

Return \mathbf{x}_0

C.3 Annealed Langevin MCMC with recurrent training-free guidance

In this section, we prove the connection between annealed Langevin MCMC (Alg. 1) and training-free guidance (Alg. 2) in Proposition. 1. We divide the proof into two parts. In Sec. C.3.1 we prove the equivalence between naive recurrence steps and Langevin MCMC. Then in Sec. C.3.2, we prove that adding the guidance term is defining an annealing path that biases towards high score regions.

C.3.1 Equivalence between Langevin MCMC and naive recurrence

Consider the diffusion process with the following stochastic interpolant [47]:

$$\mathbf{x}_t = \alpha_t \mathbf{x}_0 + \sigma_t \boldsymbol{\epsilon}.$$

We denote the score function of $q_t(\mathbf{x}_t)$ as $\nabla_{\mathbf{x}_t} \log q_t(\mathbf{x}_t) = s(\mathbf{x}_t, t)$. Recall the forward process in Eq. 1:

$$\mathbf{x}_t = \frac{\alpha_t}{\alpha_{t-1}} \mathbf{x}_{t-1} + \sqrt{\alpha_t^2 \left(\frac{\sigma_t^2}{\alpha_t^2} - \frac{\sigma_{t-1}^2}{\alpha_{t-1}^2} \right)} \boldsymbol{\epsilon}. \quad (9)$$

In a recurrence step in Line. 5, we first solve \mathbf{x}_{t-1}^i from \mathbf{x}_t^i using the learned score function $s(\mathbf{x}_t^i, t)$, then add noise to \mathbf{x}_{t-1}^i to obtain the recurrent sample \mathbf{x}_t^{i+1} , where the superscript denotes the recurrence step index: $i = 0, 1, \dots, N_{\text{recur}}$. Depending on different solvers, we have different formulations of \mathbf{x}_t^{i+1} .

DDIM sampler. When using DDIM [65] sampler, we have the reverse step as:

$$\mathbf{x}_{t-1} = \frac{\alpha_{t-1}}{\alpha_t} \mathbf{x}_t + \sigma_t^2 \left(\frac{\alpha_{t-1}}{\alpha_t} - \frac{\sigma_{t-1}}{\sigma_t} \right) s(\mathbf{x}_t, t), \quad (10)$$

where $s(\mathbf{x}_t, t)$ is the score function $\nabla_{\mathbf{x}_t} \log q_t(\mathbf{x}_t)$. Thus, we have:

$$\begin{aligned} \mathbf{x}_t^{i+1} &= \frac{\alpha_t}{\alpha_{t-1}} \mathbf{x}_{t-1}^i + \alpha_t \sqrt{\frac{\sigma_t^2}{\alpha_t^2} - \frac{\sigma_{t-1}^2}{\alpha_{t-1}^2}} \boldsymbol{\epsilon}^i \\ &= \mathbf{x}_t^i + \sigma_t^2 \left(1 - \frac{\alpha_t}{\alpha_{t-1}} \frac{\sigma_{t-1}}{\sigma_t} \right) s(\mathbf{x}_t^i, t) + \sigma_t \sqrt{1 - \frac{\alpha_t^2}{\alpha_{t-1}^2} \frac{\sigma_{t-1}^2}{\sigma_t^2}} \boldsymbol{\epsilon}^i. \end{aligned}$$

Denote $\lambda_t = \log \frac{\alpha_t}{\sigma_t}$, then we have:

$$\begin{aligned}\mathbf{x}_t^{i+1} &= \mathbf{x}_t^i + \sigma_t^2 (1 - e^{\lambda_t - \lambda_{t-1}}) s(\mathbf{x}_t^i, t) + \sigma_t \sqrt{1 - e^{2(\lambda_t - \lambda_{t-1})}} \boldsymbol{\epsilon}^i \\ &= \mathbf{x}_t^i + \sigma_t^2 (1 - e^{\lambda_t - \lambda_{t-1}}) s(\mathbf{x}_t^i, t) + \sigma_t \sqrt{(1 - e^{\lambda_t - \lambda_{t-1}})(1 + e^{\lambda_t - \lambda_{t-1}})} \boldsymbol{\epsilon}^i,\end{aligned}$$

where $1 + e^{\lambda_t - \lambda_{t-1}} \rightarrow 2$ when $T \rightarrow \infty$ and denoising step size approaches 0, as $\lambda_t - \lambda_{t-1} \rightarrow 0$.

DDPM sampler. In DDPM [26], we parametrize the posterior distribution as:

$$p_\theta(\mathbf{x}_{t-1}|\mathbf{x}_t) = \mathcal{N}(\mathbf{x}_{t-1}; \mu_\theta(\mathbf{x}_t, t), \Sigma_\theta(\mathbf{x}_t, t)), \quad (11)$$

where the posterior mean is:

$$\mu_\theta(\mathbf{x}_t, t) = \frac{\alpha_{t-1}}{\alpha_t} \mathbf{x}_t + \left(\sigma_t^2 \frac{\alpha_{t-1}}{\alpha_t} - \sigma_{t-1}^2 \frac{\alpha_t}{\alpha_{t-1}} \right) s(\mathbf{x}_t, t).$$

[26] parameterizes the posterior variance as $\Sigma_\theta(\mathbf{x}_t, t) = \beta_t \mathbf{I}$ or $\Sigma_\theta(\mathbf{x}_t, t) = \tilde{\beta}_t \mathbf{I}$:

$$\begin{aligned}\beta_t &= \alpha_t^2 \left(\frac{\sigma_t^2}{\alpha_t^2} - \frac{\sigma_{t-1}^2}{\alpha_{t-1}^2} \right), \\ \tilde{\beta}_t &= \frac{\sigma_{t-1}^2}{\sigma_t^2} \beta_t,\end{aligned}$$

while [54] propose to train the posterior variance as $\Sigma_\theta(\mathbf{x}_t, t) = \exp(v \log \beta_t + (1-v) \log \tilde{\beta}_t)$.

Thus, a backward step can be written as:

$$\mathbf{x}_{t-1} = \frac{\alpha_{t-1}}{\alpha_t} \mathbf{x}_t + \left(\sigma_t^2 \frac{\alpha_{t-1}}{\alpha_t} - \sigma_{t-1}^2 \frac{\alpha_t}{\alpha_{t-1}} \right) s(\mathbf{x}_t, t) + \Sigma_\theta^{1/2}(\mathbf{x}_t, t) \boldsymbol{\epsilon}_{\text{post}},$$

where $\boldsymbol{\epsilon}_{\text{post}}$ denotes the noise added in the posterior sampling step. Then, we can write the recurrence step as:

$$\begin{aligned}\mathbf{x}_t^{i+1} &= \mathbf{x}_t^i + \left(\sigma_t^2 - \sigma_{t-1}^2 \frac{\alpha_t^2}{\alpha_{t-1}^2} \right) s(\mathbf{x}_t^i, t) + \Sigma_\theta^{1/2}(\mathbf{x}_t^i, t) \boldsymbol{\epsilon}_{\text{post}}^i + \alpha_t \sqrt{\frac{\sigma_t^2}{\alpha_t^2} - \frac{\sigma_{t-1}^2}{\alpha_{t-1}^2}} \boldsymbol{\epsilon}_{\text{forward}}^i \\ &= \mathbf{x}_t^i + \beta_t s(\mathbf{x}_t^i, t) + \sqrt{\Sigma_\theta(\mathbf{x}_t, t) + \beta_t \mathbf{I}} \boldsymbol{\epsilon}^i,\end{aligned}$$

where $\Sigma_\theta(\mathbf{x}_t, t) \rightarrow \beta_t \mathbf{I}$ when $T \rightarrow \infty$, and the denoising step size approaches 0.

Putting together. In general, we can write the recurrence step as:

$$\mathbf{x}_t^{i+1} = \mathbf{x}_t^i + a_t s(\mathbf{x}_t^i, t) + b_t \boldsymbol{\epsilon}^i. \quad (12)$$

with $a_t \rightarrow 0$, $b_t \rightarrow 0$ and $2a_t \rightarrow b_t^2$ as the denoising step size approaches 0. Thus, it can be seen as a approximation of the ULA in Eq. 8, and also a discretization of the Langevin SDE in Eq. 7.

C.3.2 Annealed Langevin MCMC with guidance

When applying training free guidance [94] during the recurrence, we have:

$$\mathbf{x}_t^{i+1} = \mathbf{x}_t^i + a_t s(\mathbf{x}_t^i, t) + b_t \boldsymbol{\epsilon}^i + \boldsymbol{\Delta}(\mathbf{x}_t, t),$$

where a_t, b_t are the coefficients of the recurrence equation in Eq. 12 without guidance. In general, $\boldsymbol{\Delta}_t = \rho_t \nabla_{\mathbf{x}_t} \log f(\mathbf{x}_{0|t}) + \mu_t \alpha_t \nabla_{\mathbf{x}_{0|t}} \log f(\mathbf{x}_{0|t})$, where ρ_t, μ_t controls the guidance strength. We then show that the guidance term can be considered as the score function of a set of annealed verifiers

$$\left\{ \hat{f}(\mathbf{x}_t) \right\}_{t=0}^T.$$

When considering ‘variance guidance’ in Line. 7, we have $\boldsymbol{\Delta}_{\text{var}} = \rho_t \nabla_{\mathbf{x}_t} \log f(\mathbf{x}_{0|t})$. Thus, we can define $\hat{f}_t^{\text{var}}(\mathbf{x}_t) = f(\mathbf{x}_{0|t})$, which satisfies $\hat{f}_0^{\text{var}}(\mathbf{x}_0) = f(\mathbf{x}_0)$. Similarly, for ‘mean guidance’ in Line. 8, we have

$$\begin{aligned}\boldsymbol{\Delta}_{\text{mean}} &= \mu_t \alpha_t \nabla_{\mathbf{x}_{0|t}} \log f(\mathbf{x}_{0|t}) \\ &= \mu_t \frac{\sigma_t^2}{\Sigma_{0|t}} \nabla_{\mathbf{x}_t} \log f(\mathbf{x}_{0|t}),\end{aligned}$$

where the second Equation follows from Lemma 3.3 in [94]. Thus, there exists a set of functions $\hat{f}_t^{\text{mean}}(\mathbf{x}_t)$ such that $\nabla_{\mathbf{x}_t} \log \hat{f}_t^{\text{mean}}(\mathbf{x}_t) = \frac{\sigma_t^2}{\Sigma_{0|t}} \nabla_{\mathbf{x}_t} \log f(\mathbf{x}_{0|t})$, and we can see that when $t \rightarrow 0$, $\nabla_{\mathbf{x}_t} \log \hat{f}_t^{\text{mean}}(\mathbf{x}_t) = \nabla_{\mathbf{x}_0} \log f(\mathbf{x}_0)$. If we additionally incorporate the ‘implicit dynamics’ in Line. 4, our arguments still stands since the smoothed objective $\tilde{f}(\mathbf{x}) = \mathbb{E}_{\delta \sim \mathcal{N}(0, I)} f(\mathbf{x} + \bar{\gamma} \sigma_t \delta)$ converges to f with $t \rightarrow 0$ and $\sigma_t \rightarrow 0$.

Combining the two terms together, we have $\Delta_t = c_t \nabla_{\mathbf{x}_t} \log \hat{f}_t(\mathbf{x}_t)$ with $\hat{f}_t = \hat{f}_t^{\text{var}} \cdot \hat{f}_t^{\text{mean}}$. Thus, recurrence with guidance can be written as:

$$\mathbf{x}_t^{i+1} = \mathbf{x}_t^i + a_t s(\mathbf{x}_t^i, t) + b_t \epsilon^i + c_t \nabla_{\mathbf{x}_t} \log \hat{f}_t(\mathbf{x}_t),$$

which, in the continuous limit of $a_t, b_t, c_t \rightarrow 0$, converges to the Langevin SDE:

$$d\mathbf{x}_t^i = \nabla_{\mathbf{x}_t^i} \log \left(q_t(\mathbf{x}_t^i) \hat{f}_t(\mathbf{x}_t^i) \right) dt + \sqrt{2} d\mathbf{w}^i,$$

where i is the time index of recurrence steps. Thus, we have defined the annealing path as $\tilde{q}_t(\mathbf{x}_t) = q_t(\mathbf{x}_t) \hat{f}_t(\mathbf{x}_t)$, $t = 1, 2, \dots, T$.

C.4 Relationship between Langevin MCMC and gradient ascent

In training-free guidance, most prior works only apply gradient ascent without recurrence. Here we provide a theoretical analysis of both methods.

Recall the KL-divergence objective in Eq. 5, which can be further decomposed when we are sampling from a compositional distribution of $p_0(\mathbf{x}_0)$ and verifier $f(\mathbf{x}_0)$, with $\nu \propto p_0 \cdot f$:

$$H_\nu(\rho) = \mathbb{E}_\rho[-\log f] + H_{p_0}(\rho) + \log Z.$$

where $Z = \int p_0 f$ is a normalization constant. Thus, gradient ascent is optimizing the verifier objective $\mathbb{E}_\rho[-\log f]$, while Langevin MCMC in Eq. 12 is optimizing the divergence between current sample and base distribution $H_{p_0}(\rho)$. This explains why naive gradient updates leads to OOD samples, and recurrence effectively mitigates this issue, acting as a contraction force pulling the sample back to the original manifold. However, since we start from p_0 as the distribution of our initial sample, sometimes we can omit the recurrence if the guidance strength is small. But if we wish to traverse different modes with multiple gradient updates, introducing recurrence helps to avoid OOD during optimization.

C.5 Implementing Local Search with TFG hyper-parameter space

Due to the equivalence between annealed Langevin MCMC and training-free guidance with recurrence, we can implement local search with Langevin MCMC using the TFG framework of [94], efficiently searching the hyperparameters. Here we provide an overview of the algorithm and design space. Following Sec. C.3, every iteration of recurrence in Line. 5 is equivalent to an annealed Langevin MCMC step, thus N_{recur} is equal to the number of local search steps.

For time varying schedules ρ_t, μ_t , we follow [94] and propose to use either the ‘increase’ schedule:

$$s_t = T \frac{\alpha_t / \alpha_{t-1}}{\sum_{t=1}^T \alpha_t / \alpha_{t-1}}, \quad (13)$$

where we increase the guidance strength as we denoise: $s_T < s_{T-1} < \dots < s_1$; or the ‘constant’ schedule

$$s_t = 1, \quad (14)$$

which uses constant parameters throughout the denoising process. Thus, the time-varying schedules can be computed as $\rho_t = s_t \bar{\rho}$ and $\mu_t = s_t \bar{\mu}$, and we only need to determine the average $\bar{\rho}$ and $\bar{\mu}$.

D Global Search of Denoising Diffusion Models

In this section, we provide details about the global search algorithms: BFS and DFS.

Algorithm 2 Training-Free Guidance

```

1: Input: Unconditional diffusion model  $\epsilon_\theta$ , verifier  $f$ , guidance strength  $\rho, \mu, \bar{\gamma}$ , number of steps
    $T, N_{\text{recur}}, N_{\text{iter}}$ 
2:  $\mathbf{x}_T \sim \mathcal{N}(\mathbf{0}, \mathbf{I})$ 
3: for  $t = T, \dots, 1$  do
4:   Define function  $\tilde{f}(\mathbf{x}) = \mathbb{E}_{\delta \sim \mathcal{N}(\mathbf{0}, \mathbf{I})} f(\mathbf{x} + \bar{\gamma} \sigma_t \delta)$ 
5:   for  $r = 1, \dots, N_{\text{recur}}$  do
6:      $\mathbf{x}_{0|t} = (\mathbf{x}_t - \sigma_t \epsilon_\theta(\mathbf{x}_t, t)) / \alpha_t$ 
7:      $\Delta_{\text{var}} = \rho_t \nabla_{\mathbf{x}_t} \log \tilde{f}(\mathbf{x}_{0|t})$ 
8:      $\Delta_{\text{mean}} = \Delta_{\text{mean}} + \mu_t \alpha_t \nabla_{\mathbf{x}_{0|t}} \log \tilde{f}(\mathbf{x}_{0|t} + \Delta_{\text{mean}})$   $\triangleright$  Iterate  $N_{\text{iter}}$  times starting from  $\Delta_{\text{mean}} = \mathbf{0}$ 
9:      $\mathbf{x}_{t-1} = \text{Sample}(\mathbf{x}_t, \mathbf{x}_{0|t}, t) + \frac{\alpha_{t-1}}{\alpha_t} (\Delta_{\text{var}} + \Delta_{\text{mean}})$   $\triangleright$  Sample follows DDIM or DDPM
10:     $\mathbf{x}_t \sim \mathcal{N}\left(\frac{\alpha_t}{\alpha_{t-1}} \mathbf{x}_{t-1}, \alpha_t^2 \left(\frac{\sigma_t^2}{\alpha_t^2} - \frac{\sigma_{t-1}^2}{\alpha_{t-1}^2}\right) \mathbf{I}\right)$   $\triangleright$  Recurrent strategy
11:   end for
12: end for
13: Output: Conditional sample  $\mathbf{x}_0$ 

```

D.1 BFS-Based Search

We present the pseudo code for BFS in Alg. 3. The core hyperparameters of BFS are the temperature τ_t and the evaluation time steps \mathcal{S} . These parameters enable a smooth transition from Best-of-N to best-first search. In general, a higher τ_t and evaluation at earlier time steps bias the process toward high-score samples, while a lower temperature and evaluation at later (smaller) time steps approximate the Best-of-N approach.

In practice, we typically evaluate at fractions of the sampling steps, with $\mathcal{S} = \{\frac{3}{4}T, \frac{1}{2}T, \frac{1}{4}T\}$. We perform a grid search over the temperature values to determine an appropriate magnitude using a small number of particles, and then apply this configuration when scaling up the number of particles. We use the ‘increase’ schedule in Eq. 13 for τ_t , so that $\tau_T \leq \tau_{T-1} \leq \dots \leq \tau_0$, reflecting increased confidence in the verifier evaluation at smaller time steps.

D.2 DFS-based search

In this section, we provide the details and pseudo code for DFS in Alg. 4. To better utilize previously explored sampling paths, we employ a buffer to store prior results. When no particles pass the threshold constraint, we retrieve the best sample from the buffer.

Similar to BFS, controlling the set of evaluation steps allows a trade-off between efficiency and accuracy. Evaluating at earlier time steps introduces higher uncertainty but enables earlier resampling. Additionally, adjusting the backtracking depth Δ_T governs the search scope: a small Δ_T reduces computation and favors local search, while a larger Δ_T enables broader exploration at the cost of increased computation.

In practice, we set the evaluation steps to $\mathcal{S} = \{\frac{1}{2}T, \frac{1}{4}T\}$ for image experiments to save compute, and to $\mathcal{S} = \{\frac{3}{4}T, \frac{3}{4}T - 1, \dots, 1\}$ for PointMaze experiments. We set the recurrence depth to $T/2$ for image tasks and $T/4$ for PointMaze, corresponding to the denoised steps at which samples are first evaluated. The threshold schedule δ_t is also set to ‘increase’ as in Eq. 13, enforcing tighter constraints for samples with lower noise.

In our experiments, we observed that when backtracking to $t_{\text{next}} = T$ —thus fully restarting—the nonzero terminal SNR α_T / σ_T in many diffusion schedules [40] can lead to cumulative errors with repeated backtracking. Therefore, when backtracking to $t_{\text{next}} = T$, we initialize with fresh Gaussian noise.

E Experiment Details

In this section we provide the details of experimental setup and implementation for all our experiments. We run our experiments on clusters with Nvidia A100 GPUs, with over 1000 GPU hours used.

Algorithm 3 Diffusion BFS

Diffusion input: diffusion model ϵ_θ with diffusion time steps T and proposal transition kernel $\{\tilde{p}_\theta(\mathbf{x}_{t-1}|\mathbf{x}_t)\}_{t=1}^N$. Verifier f .
BFS input: Set of evaluation time steps \mathcal{S} . Temperature schedule τ_t . Budget of particles K .
Init: Random sample K particles $\mathbf{x}_T^k \sim \mathcal{N}(\mathbf{0}, \mathbf{I})$, $k = 1, 2, \dots, K$. Set the number of particles $K_T = K$.
for $t = T, \dots, 1$ **do**
 if $t \in \mathcal{S}$ **then**
 for $k = 1, 2, \dots, K_t$ **do**
 Estimate the conditional mean: $\mathbf{x}_{0|t}^k = \frac{\mathbf{x}_t^k - \sigma_t \epsilon_\theta(\mathbf{x}_t^k, t)}{\alpha_t}$. Compute the verifier score $f(\mathbf{x}_{0|t}^k)$.
 Compute the number of children n_t^k :
 if Resample **then**
 $n_t^k = \text{Round} \left(K_t \frac{f(\mathbf{x}_{0|t}^k)^{\tau_t}}{\sum_{i=1}^{K_t} f(\mathbf{x}_{0|t}^i)^{\tau_t}} \right)$
 else if Prune **then**
 $n_t^k = \min \left(1, \text{Round} \left(K_t \frac{f(\mathbf{x}_{0|t}^k)^{\tau_t}}{\sum_{i=1}^{K_t} f(\mathbf{x}_{0|t}^i)^{\tau_t}} \right) \right)$
 end if
 end for
 else
 $n_t^k = 1$
 end if
 for $k = 1, \dots, K_t$ **do**
 Sample n_t^k particles from \mathbf{x}_t^k : $\mathbf{x}_{t-1}^j \sim \tilde{p}_\theta(\cdot|\mathbf{x}_t^k)$, $j = 1, 2, \dots, n_t^k$
 end for
 The number of particles at next noise level: $K_{t-1} = \sum_{k=1}^{K_t} n_t^k$
end for
Return $\mathbf{x}_0 = \text{argmax}_{k=1, \dots, K_0} f(\mathbf{x}_0^k)$

Algorithm 4 Diffusion DFS

Diffusion input: diffusion model ϵ_θ with diffusion time steps T and proposal transition kernel $\{\tilde{p}_\theta(\mathbf{x}_{t-1}|\mathbf{x}_t)\}_{t=1}^N$. Verifier f .
DFS input Budget for total number of backtracking $B = K$, backtracking depth Δ_T and threshold $\{\delta_t\}_{t=1}^T$. Set of evaluation time steps \mathcal{S} .
Init $\mathbf{x}_T \sim \mathcal{N}(\mathbf{0}, \mathbf{I})$, $t = T$. Init buffer with empty sets: $\text{buffer}(t) \leftarrow \{\}$, $t = 1, 2, \dots, T$.
while $t > 0$ **do**
 if $t \in \mathcal{S}$ **then**
 Estimate the conditional mean and verifier score: $\mathbf{x}_{0|t} = \frac{\mathbf{x}_t - \sigma_t \epsilon_\theta(\mathbf{x}_t, t)}{\alpha_t}$, $f(\mathbf{x}_{0|t})$.
 if $f(\mathbf{x}_{0|t}) < \delta_t$ and budget $B > 0$ **then**
 Backtrack: $t_{\text{next}} \leftarrow \min(t + \Delta_T, T)$, $\mathbf{x}_{t_{\text{next}}} \sim q(\mathbf{x}_{t_{\text{next}}}|\mathbf{x}_t)$ with q in Eq. 1
 Decrease the budget: $B \leftarrow B - 1$
 Add the score-value pair to the buffer: $\text{buffer}(t).add(f(\mathbf{x}_{0|t}) : \mathbf{x}_t)$
 else
 if $f(\mathbf{x}_{0|t}) < \delta_t$ and budget $B = 0$ **then**
 Pop the best sample from buffer: $\mathbf{x}_t \leftarrow \text{buffer}(t).max \quad \triangleright \text{select the best sample from past explorations}$
 end if
 Sample posterior: $t_{\text{next}} \leftarrow t - 1$, $\mathbf{x}_{t_{\text{next}}} \sim \tilde{p}_\theta(\mathbf{x}_{t-1}|\mathbf{x}_t)$
 end if
 else
 Sample posterior: $t_{\text{next}} \leftarrow t - 1$, $\mathbf{x}_{t_{\text{next}}} \sim \tilde{p}_\theta(\mathbf{x}_{t-1}|\mathbf{x}_t)$
 end if
 $t \leftarrow t_{\text{next}}$, $\mathbf{x}_t \leftarrow \mathbf{x}_{t_{\text{next}}}$
end while
Return \mathbf{x}_0

E.1 Long Horizon Maze Planning

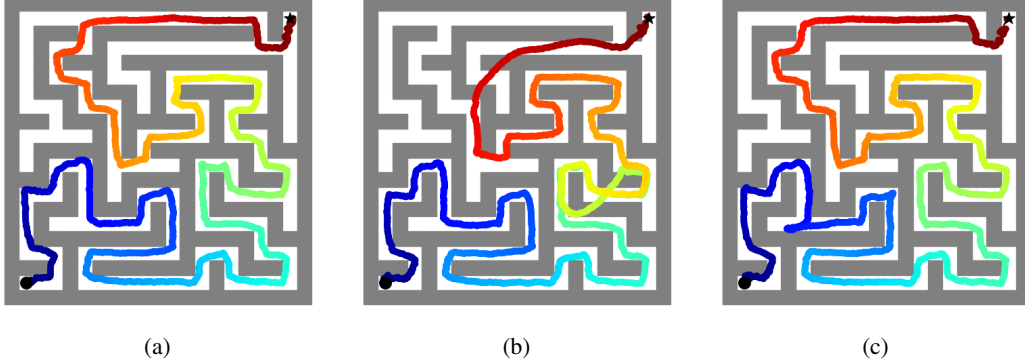


Figure 6: **Additional examples for PointMaze Ultra** Fig. 6a shows the maze layout and an example trajectory rollout. Fig. 6b shows the failure case of model-generated plan. Fig. 6c shows a successful generated plan after inference-time scaling.

Maze environment. For all our maze experiments we use the OGBench PointMaze [55]. PointMaze Giant was directly adapted from their datasets, and we create PointMaze Ultra using the same protocol of Figure 5 in [49]², but with a smaller size of 20x20 cells. Dataset for Ultra is collected following the protocol in OGBench [55]. A larger layout and example trajectory of PointMaze Ultra is shown in Fig. 6. We evaluate the model on the default task 1 of OGBench [55], which is navigating from bottom left to top right. Empirically we discover that the diffusion model can perform well on short-horizon tasks without extra inference compute, but struggles heavily in the long horizon tasks.

Model Training. We train the model following diffuser [31], where we use a temporal U-Net to denoise the trajectory. Since our objective start and goal is more distant than trajectories in dataset, we sample at longer horizons than training, which is enabled by the temporal U-Net architecture. Specifically, for PointMaze Giant, we train at horizon 400 and sample at 600; and for PointMaze Ultra, we train at horizon 2000 and sample at 2800. For the PointMaze Ultra model we extend the depth of the U-Net for 1 more layer, and keep all other parameters the same. We train the model for 1.2M steps using the same configuration as [31].

Inference. We found that the model performance saturates with 16 denoising steps, which we use for all our experiments. For all the data points we report the average success rate with over 40 samples.

For verifier design, we use the ground-truth maze layout, and calculate the violation of each point in the trajectory using the position coordinates. Specifically, if a point (x, y) is inside a maze wall box with center (c_x, c_y) and half-width d , then the point loss can be calculated as the minimum distance from the point to box walls:

$$L(x, y) = \min(x - (c_x - d), (c_x + d) - x, y - (c_y - d), (c_y + d) - y) .$$

and the total verifier score is computed as:

$$f(\tau) = \exp \left(- \sum_{i=1}^H L(x_i, y_i)^2 \right) .$$

So if all the points are free of violation in the trajectory, then $f(\tau) = 1$. We point out that this does not indicate a successful plan as the connection between consecutive points $(x_i, y_i) \rightarrow (x_{i+1}, y_{i+1})$ may violate the maze layout, and using only the verifier function can not generate a successful plan.

For local search, we search the hyper-parameters $\bar{\rho}$ and $\bar{\mu}$ in Sec. C.5 with $\bar{\gamma} = 0$, and we set the local search steps (recurrence steps) to 2 for Giant and 6 for Ultra. We set $N_{\text{iter}} = 1$ as we observe they do not contribute to the performance gains, while the number of Langevin MCMC steps has the most impact on performance. For global search with BFS we evaluate at steps $\{12, 8, 4\}$, and for DFS we evaluate at $\{12, 11, \dots, 1\}$ with backtracking depth $\Delta_T = 4$. We also observe that

²<https://github.com/mpetersen94/gcs/blob/main/models/maze.py>

increasing backtracking depth to 12 and evaluate at smaller time steps $\{4, 3, 2, 1\}$ helps to scale up the performance with more compute. We use grid search to determine temperature and threshold, with a step size of $[1, 5, 10]$ for each magnitude.

E.2 Offline RL

Setup. We follow the setup in [44], and we directly use their pretrained diffusion model and Q-function, omitting the time-dependent energy function. The diffusion model was trained to generate action \mathbf{a} given state \mathbf{s} , and we sample with 15 steps of DDIM.

For hyper-parameter search, we disable the implicit dynamics and set $\bar{\gamma} = 0$, and use the ‘increase’ schedule for ρ and μ . For strength parameters $\bar{\rho}$ and $\bar{\mu}$, we first search for the right magnitude. Then, we also follow [44] and search with step size $[1, 2, 3, 5, 8, 10]$ within the magnitude. Same as [44], we use 5 different seeds with 10 samples per seed for each task. To avoid over fitting, we use different seeds for parameter search and evaluation. We report the hyper-parameters and the performance within the parameter-searching dataset and evaluation dataset.

For global search, we use 4 particles for Medium-Expert and Medium datasets, and 2 particles for Medium-Replay datasets. Since the number of particles are small, we do not carry out BFS or DFS methods and simply use Best-of-N. We point out that the number of particles we use are much smaller than the 50 particles in [80] and the 32 particles in [8], highlighting the effectiveness of local search.

Baseline. We compare our method to a variety of baselines, including traditional state-of-the-art methods like CQL [35], BCQ [20] and IQL [34], diffusion-based policies such as diffuser [31], decision-diffuser (DD) [1], Diffusion-QL (D-QL) [80], SfBS [8] and QGPO [44]. We directly take the numbers from [44].

Among the baseline diffusion-based methods, both Diffuser [31] and QGPO [44] requires training a noise-dependent guidance function, and D-QL [80] requires updating the diffusion model during training using the Q-function iteratively, which needs to back-propagate through the diffusion sampling chain, introducing high computation and memory overheads. DD [1] uses classifier-free guidance [27] to generate high-return trajectories, which requires training a return-conditional model on labeled datasets, which can be expensive to obtain in robotics where only demonstration data is available [43].

Dataset	Environment	particles	N_{recur}	N_{iter}	$\bar{\rho}$	$\bar{\mu}$	Eval set	Search set
Medium-Expert	HalfCheetah	4	1	1	0.008	0.02	93.9 ± 0.3	94.3 ± 0.5
Medium-Expert	Hopper	4	1	4	0.001	0.00	104.4 ± 3.1	109.4 ± 5.2
Medium-Expert	Walker2d	4	1	1	0.005	0.10	111.4 ± 0.1	111.4 ± 0.2
Medium	HalfCheetah	4	1	4	0.003	0.05	54.8 ± 0.1	54.8 ± 0.2
Medium	Hopper	4	4	4	0.003	0.02	99.5 ± 1.7	100.1 ± 0.1
Medium	Walker2d	4	1	6	0.003	0.08	86.5 ± 0.2	85.2 ± 3.2
Medium-Replay	HalfCheetah	2	1	6	0.005	0.03	47.8 ± 0.4	48.4 ± 0.1
Medium-Replay	Hopper	2	1	1	0.003	0.20	97.4 ± 4.0	100.4 ± 2.2
Medium-Replay	Walker2d	2	2	4	0.003	0.03	79.3 ± 9.7	83.2 ± 2.8
Average							86.1	87.5

Table 3: Hyper-parameters on D4RL locomotion tasks with test-time scaling. We report the performance on hyper-parameter search dataset and the evaluation dataset, highlighting the best number.

E.3 Image Generation

E.3.1 Text-to-Image Compositional Generation

Setup. We use the SSD-1B model³ which is distilled from SDXL, and we use the default sampling configuration with 50 steps of DDIM sampler. We use the oracle verifier of each task following CompBench [29].

³<https://huggingface.co/segmind/SSD-1B>

Global search with DFS. For DFS we evaluate at time steps $\{25, 35, 45\}$ and set the backtrack depth $\Delta_T = 25$. We set the threshold for our experiments to 0.5, 0.7 and 0.9, with the ‘constant’ schedule in Eq. 14. We typically use a higher threshold for high computation budgets, representing using more compute for higher quality standard.

We provide example visualizations in Fig. 7.

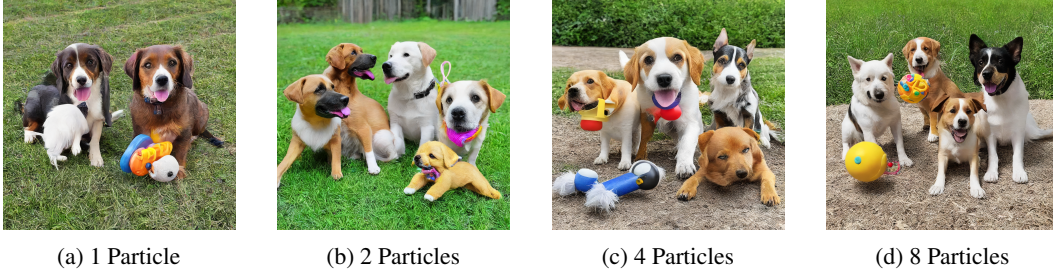


Figure 7: **Example of inference-time scaling with Numeracy dataset** Above shows the results of Best-of-N with different particles, with prompt: “four dogs played with two toys”

E.3.2 ImageNet Conditional Generation

Setup. We use the 256x256 DDPM ImageNet model from [12], and for local search we use the 224px ViT classifier⁴ and for global search we use the 384px version⁵ when using double-verifier. We evaluate on class label 222 and 444, with 256 samples per label. We sample with 100 DDPM steps. When evaluating the class accuracy we use the DeiT model⁶, and we evaluate the FID against the images of the corresponding class in ImageNet.

Global search with BFS. Due to computation constraints we set the local search steps to 1 in all experiments. For BFS we set the evaluation steps as $\{75, 50, 25\}$, and use $\bar{\tau} = 1.0$ for label 222 and $\bar{\tau} = 0.5$ for label 444 with the ‘increase’ schedule.

We provide example visualizations in Fig. 8.

⁴<https://huggingface.co/google/vit-base-patch16-224>

⁵<https://huggingface.co/google/vit-base-patch16-384>

⁶<https://huggingface.co/facebook/deit-small-patch16-224>



(a) 2 Particles



(b) 4 Particles



(c) 8 Particles



(d) 12 Particles

Figure 8: Visualizations of ImageNet Conditional Generation Above shows the uncured samples for class label 222 with BFS with different number of particles